



**HAL**  
open science

## **Sedimentary stylolite networks and connectivity in Limestone: Large-scale field observations and implications for structure evolution**

Leehee Laronne Ben-Itzhak, Einat Aharonov, Ziv Karcz, Maor Kaduri,  
Renaud Toussaint

### ► To cite this version:

Leehee Laronne Ben-Itzhak, Einat Aharonov, Ziv Karcz, Maor Kaduri, Renaud Toussaint. Sedimentary stylolite networks and connectivity in Limestone: Large-scale field observations and implications for structure evolution. *Journal of Structural Geology*, 2014, pp.online first. 10.1016/j.jsg.2014.02.010 . hal-00961075v1

**HAL Id: hal-00961075**

**<https://hal.science/hal-00961075v1>**

Submitted on 19 Mar 2014 (v1), last revised 19 Mar 2014 (v2)

**HAL** is a multi-disciplinary open access archive for the deposit and dissemination of scientific research documents, whether they are published or not. The documents may come from teaching and research institutions in France or abroad, or from public or private research centers.

L'archive ouverte pluridisciplinaire **HAL**, est destinée au dépôt et à la diffusion de documents scientifiques de niveau recherche, publiés ou non, émanant des établissements d'enseignement et de recherche français ou étrangers, des laboratoires publics ou privés.

1  
2 **Sedimentary stylolite networks and connectivity in**  
3 **Limestone: Large-scale field observations and**  
4 **implications for structure evolution**

5  
6 Laronne Ben-Itzhak L.<sup>1</sup>, Aharonov E.<sup>1</sup>, Karcz Z.<sup>2,\*</sup>,

7 Kaduri M.<sup>1,\*\*</sup> and Toussaint R.<sup>3,4</sup>

8  
9 <sup>1</sup> *Institute of Earth Sciences, The Hebrew University, Jerusalem, 91904, Israel*

10 <sup>2</sup> *ExxonMobil Upstream Research Company, Houston TX, 77027, U.S.A*

11 <sup>3</sup> *Institut de Physique du Globe de Strasbourg, University of Strasbourg/EOST, CNRS, 5 rue*  
12 *Descartes, F-67084 Strasbourg Cedex, France.*

13 <sup>4</sup> *Centre for Advanced Study at The Norwegian Academy of Science and Letters, Drammensveien*  
14 *78, 0271 N-Oslo, Norway.*

15  
16 \* *Currently at Delek Drilling LP*

17 \*\* *Currently at ISTERre, University J. Fourier – Grenoble I, BP 53, F-38041 Grenoble, France*

18

19

20

21

## 22 **Abstract**

23       Stylolites are rough surfaces, formed by localized rock dissolution, and prevalent in  
24 carbonates and other sedimentary rocks. Their impact on porosity and permeability, and capacity  
25 to accommodate compactive strain, are well documented. This paper presents a meso-scale field  
26 study on sedimentary stylolites in carbonates, characterizing large-scale distributions of  
27 stylolites, including measurements conducted on longer than kilometer-long stylolites. Our field  
28 study suggests that on large-scales connections between stylolites become important. Since  
29 connectivity, and also lack of connectivity, are expected to play a significant role in strain  
30 accommodation and hydraulic rock properties, we suggest that large-scale analysis may require a  
31 new characterization scheme for “stylolites populations”, based on their connectivity. We  
32 therefore divide sedimentary stylolite populations into three end-member types, which are  
33 correlated with the three possibilities for percolation of such systems: isolated stylolites (with  
34 zero percolation/connectivity), long-parallel stylolites (with 2-dimensional  
35 percolation/connectivity), and interconnected stylolite networks (with 3-dimensional  
36 percolation/connectivity). New statistical parameters and measures are devised and used to  
37 quantitatively characterize the different population types. Schematic mechanistic models are then  
38 offered to explain the evolution of the three end-member connectivity-classes. In addition we  
39 discuss the effect on fluid flow of the different population types.

40

41

42

## 43 **1. Introduction**

44

45 Stylolites are rough surfaces of dissolution, common in sedimentary rocks and especially  
46 prominent in carbonates. They are lined by a thin layer of relatively insoluble particles, mainly  
47 clay minerals, oxides, and organic matter, that are thought to accumulate while the major  
48 constituent of the rock, which is more soluble (e.g. carbonate, quartz) dissolves away (Stockdale,  
49 1922, Park and Schot, 1968, Kaplan, 1976, Railsback, 1993). Stylolites are known to affect fluid  
50 flow in opposing ways: On the one hand, stylolites are often associated with reduced  
51 permeability - material that dissolves at the stylolite precipitates in adjacent pores, forming  
52 “tight” units (Wong and Oldershaw, 1981, Tada and Siever, 1989, Finkel and Wilkinson, 1990,  
53 Ehrenberg, 2006) that are important in management of hydrocarbon aquifers and reservoirs  
54 (Corwin et al., 1997). In other cases, stylolites may enhance porosity and permeability in their  
55 vicinity, in particular their tips (Carozzi and Vonbergen, 1987, Raynaud and Carrioschaffhauser,  
56 1992) and sometimes fluid flow is observed along stylolitic surfaces (Wong and Oldershaw,  
57 1981, Rye and Bradbury, 1988, Heap et al., 2014). In addition to their hydraulic role, stylolites  
58 are also known to accommodate large compactive strains (Tada and Siever, 1989), playing a key  
59 role in the evolution of mechanical rock properties, and the overall compactive strain of rocks.

60

61 Stylolite formation is attributed to localized Pressure Solution (PS). PS is broadly defined as  
62 dissolution and re-precipitation driven by spatial variations in chemical potential along grain  
63 surfaces: regions with high chemical potential dissolve, the dissolved material is transported  
64 through the fluid phase, and precipitates in regions where the chemical potential is lower.  
65 Variations in the chemical potential arise due to spatial variations in stress, plastic and elastic  
66 strain energies, crystal orientation and interface curvature (Deboer, 1977, Lehner, 1995,  
67 Paterson, 1995, Shimizu, 1995). The chemical potential can be extended to an electrochemical

68 potential (Greene et al., 2009) where spatial variations in surface charge are considered as well.  
69 Clays and organic matter are also thought to play an important role in the PS process (Heald,  
70 1956, Thomson, 1959, Sibley and Blatt, 1976, Gruzman, 1997), and their distribution and  
71 content are believed to affect the rate of PS (Hickman and Evans, 1995, Renard et al., 2001) and  
72 the degree of PS localization on stylolites (Heald, 1955, 1956, Engelder and Marshak, 1985,  
73 Marshak and Engelder, 1985). How clays, phyllosilicates, and organic matter enhance PS is not  
74 fully understood, and suggestions include purely physical (propping grain contacts) (Weyl,  
75 1959), chemical (varying pH) (Thomson, 1959), electrochemical (solute gradients amplified by  
76 clay electric charge) (Walderhaug et al., 2006) effects, or a combination of the above.

77 Key models for stylolite formation view them as isolated and spatially limited surfaces (e.g.  
78 Fletcher and Pollard (1981); Stockdale (1922)). However, in the field they are rarely “isolated”,  
79 but rather appear to be closely related to other stylolites and structures (primarily Mode I and  
80 Mode II fractures) (Peacock and Sanderson, 1995, Smith, 2000). Perhaps because of the scarcity  
81 of isolated stylolites, and the difficulty in determining their terminations when not isolated, there  
82 is very limited literature on stylolites' lateral extent. Stylolites were traced in limestone for over  
83 50 m by Park and Schot (1968), and Safaricz (2002) followed single stylolites for 8.5m and  
84 dissolution seams for over 800 m. An often-cited linear relationship between stylolite length and  
85 thickness (either amplitude or seam thickness), is thus based on a handful of field studies  
86 (Stockdale, 1922, Mardon, 1988, Benedicto and Schultz, 2010, Nenna and Aydin, 2011) though a  
87 theoretical rationale for it is fairly well understood (Aharonov and Katsman, 2009).

88 Most stylolites seem to have been studied on "small" outcrops or, in the case of the oil and  
89 gas industry, on cores. A few exceptions are the field-wide studies of (Stockdale, 1922,  
90 Railsback, 1993, Andrews and Railsback, 1997, Safaricz, 2002, Safaricz and Davison, 2005).  
91 Stylolites, like fractures, are "very large" in one dimension but "very small" in another  
92 dimension. Their thickness is of the order of centimeters at most, so they are impossible to  
93 resolve with standard seismic techniques. In order to determine the large-scale distribution of

94 stylolites (needed to assess for example reservoir performance or compactive basin-scale strain)  
95 the geometry and hydraulic properties of the centimeter-scale observation made routinely on  
96 cores needs to be upscaled to the kilometer-scale structure, which is always a challenging task.  
97 To devise a robust upscaling methodology, the cm-scale structure needs to be linked to the km-  
98 scale structure through an adequate analog-outcrop, as is common in the petroleum industry.  
99 Only through such an analog can upscaling parameters and workflows be tested and confirmed.  
100 Such studies were previously done on fractures (Dawers et al., 1993, Main, 1996, Cello, 1997,  
101 Willemse, 1997, Bour and Davy, 1998, McLeod et al., 2000), and led to basic understanding  
102 regarding the relationship between aperture and length (Vermilye and Scholz, 1995) and the  
103 formation and connectivity of fractures (Segall and Pollard, 1980, Cartwright et al., 1995, Gupta  
104 and Scholz, 2000). The present work performs a similar multi-scale study on sedimentary  
105 stylolites populations, aiming to quantify their distributions and connectivity and provide a step  
106 towards understanding their large-scale effects.

107

108       The connectivity of stylolites may be important both when they act as flow conduits, and in  
109 the opposite case, when they act as barriers. Their impact on large-scale flow properties can be  
110 understood using ideas from percolation theory (for a review on percolation see e.g. Bunde and  
111 Havlin (1991)). Percolation theory is a mathematical theory that addresses the question of the  
112 connectivity and conductivity within a composite material, composed of “black” defects placed  
113 within a “white” matrix. In the percolation “game” the black defects are typically assigned a  
114 different conductivity than their host white matrix, and percolation theory predicts electrical  
115 conductivity and resistivity of the composite black-white material (e.g. McLachlan et al. (1990)).  
116 The black defects are said to “percolate” when one can trace along black parts only (without  
117 “stepping” into white parts) from any side of the matrix body to any other. When black defects  
118 are conductive “percolation” is accompanied by abrupt enhancement of the conductivity of the  
119 matrix relative to a state of no percolation. The opposite game is just as simple – if black defects

120 have high resistivity (low conductivity), percolation of conducting whites controls conductivity.  
121 Percolation of conduction whites is lost when there are enough black defects, or when blacks are  
122 distributed in such a way that whites are disconnected.

123 In line of the above percolation picture, we suggest to envision stylolites as “penny-shaped”  
124 surfaces with a different fluid conductivity (higher or lower) than their host rock. These surfaces  
125 can have different radii and they can be oriented in different angles to each other and can be  
126 envisioned as “black” defects in a “white” host rock.

127

128 Percolation or connectivity of the stylolite surfaces are then expected to occur in one of three  
129 end-member ways:

130 **I: Isolated surfaces – no percolation:** If the radii of surfaces is small, and if there are not many  
131 surfaces within the region, then the surfaces may not cross each other and remain isolated from  
132 one another. In that case there is no percolation of surfaces from any side of the box to any other.  
133 This system is below the percolation threshold.

134 **II: Parallel surfaces - 2D percolation:** if surfaces are virtually infinite and parallel, they create a  
135 layered structure. In this case both surfaces and host rock percolate in the direction parallel to the  
136 surfaces, but neither of them percolates in the direction perpendicular to the surfaces. If the  
137 surfaces have higher conductivity than the host rock they will enhance conductance in the  
138 surface-parallel direction and will not affect the perpendicular direction. Instead, if the surfaces  
139 have lower conductivity they will not affect the surface-parallel direction yet will act as barriers  
140 for conductance in the perpendicular direction. In this case percolation is anisotropic and so is  
141 conductance.

142 **III: Networks of interconnected surfaces - 3D percolation:** when there are enough surfaces, and  
143 they have a distribution of orientations, they will connect to one another and allow percolation in  
144 all three dimensions.

145

146 In order to analyze the 3D connectivity of stylolites with the above framework in mind we  
147 devised new statistical characterization tools that quantify the morphology of stylolite  
148 populations. We use our new tools in three well-exposed localities, chosen from a collection of  
149 17 field-sites (Table 1). These sites were chosen due to their good exposure, and also because  
150 they exemplify the 3 end-member surface-connectivity/percolation possibilities presented above.  
151 The Supplementary provides location, geological setting and general description of stylolites  
152 exposed in the other 14 localities. Most of these are field-sites that we studied and a few are  
153 places described in the literature and studied by others.

154

## 155 **2. Methods**

156

### 157 **2.1 Field sites**

158 Three well-exposed "type" localities (1-3 in Table 1) that display possible connectivity end-  
159 member behaviors were chosen out of 17 sites (see the Supplementary Material). Detailed  
160 measurements were made in these three localities. A Bedding-parallel population of very long  
161 stylolites is studied in the Blanche cliff site to represent 2D percolation. To represent 3D  
162 percolation an anastomosing network of stylolites is analyzed in the Mitzpe Ramon quarry and a  
163 more complicated case, with a *stylolite-fracture network* that has also several *long-parallel*  
164 *stylolites* was investigated on an Umbria-Marche slab. *Isolated stylolites*, representing a non-  
165 percolating population, were not found in our field sites (as seen in Table 1). Their scarcity is  
166 explained in the discussion, while here this connectivity class is discussed based on few  
167 examples from the literature, because topologically it is an end-member scenario, even if not  
168 commonly found in the field. The three key field localities we study are described in detail  
169 below, while the other sites are referred to in the Supplementary Material.

170



**Table 1:** Field locations, which were studied as part of this work (1-13) and collected from the literature (14-17). Detailed description and photographs are presented in the text and in the Supplementary material. Class II: Long-parallel stylolites, Class IIIa: Anastomosing stylolite network, Class IIIb: stylolite-fracture network

#	Site	Location	Geological data	Population class
1	Blanche cliff	N33°12' E35°33'	Ein-El-Assad Formation (Albian), biomicritic limestone	II
2	Mitzpe Ramon (quarry) (unit U1)	N30°38' E34°48'	Avnon formation (Upper Cenomanian), bioclastic limestone.	IIIa
3	Umbria-Marche, Italy, (purchased slab)	N43° E13°	Calcare Massiccio (CM) Formation (Lower Jurassic). Wackestone–packstone limestone.	IIIb + several II
4	Mitzpe Ramon (quarry) 4 units (other than unit U1)	N30°38' E34°48'	Avnon formation (Upper Cenomanian), bioclastic limestone.	Different units: 1 unit contains IIIb, and 3 units of IIIa.
5	Nahf (quarry)	N32°56' E35°19'	Bina formation (Turonian).	II with IIIa appearing in between
6	Ein El-Assad (cliff)	N32°56' E35°23'	Ein-El-Assad Formation (Albian).	II with IIIa appearing in between
7	Tsavoia anticline (roadcut)	N30°58' E34°46'	Nezer Formation (Turonian), biomicritic limestone interlayered with dolomite and marl	II (some connections at large scales)
8	Rama (cliff)	N32°56' E35°21'	Rama Formation (Albian), limestone interlayered with marl.	IIIa
9	Machtsh Katan (exposure)	N30°57' E35°13'	Shivta and Nezer formations (Turonian)	IIIb
10	Maale Yair, Dead Sea (exposure)	(N31°12' E35°21')	Shivta formation (Turonian)	IIIa
11	State Collage, Pennsylvania (roadcut)	(N40°47' W77°48')	Devonian-Silurian limestone	II
12	Morocco (exposure)	??	??	II
13	Givat Ram, Jerusalem		Cenomanian (?), limestone	IIIa with some localities of IIIb
14 <sup>[1]</sup>	Flamborough Head, Yorkshire, UK	between Sewerby / Bridlington and High Stacks	Cretaceous chalk	IIIa and II
15 <sup>[2]</sup>	Yazd Block quarry, Esfahan Province, Central Iran	(N33°27' E54°22')	Haftoman Formation (Upper Cretaceous), limestone	IIIa
16 <sup>[3]</sup>	Illinois Basin Salem Limestone	Two coadcuts: N38°53' W86°31' and N38°32' W90°24'	Mississippian Salem limestone	II and IIIa
17 <sup>[4]</sup>	Selinsgrove Junction, Pennsylvania (creek bed exposure)	N40°47' W76°50'	Selinsgrove member, Onandaga fm (Devonian), fine-grained limestone	tectonic isolated as well as networks of (“composite-”) solution seams

171 **Blanche cliff (Fig 1):** Stylolites are exposed in the “Blanche” cliff of the Albian-age Ein-El-  
172 Assad Formation in Northern Israel. The "Blanche" here consists of a ~50m-thick biomicritic,  
173 shallow inner-platform limestone, that dips gently to the west (Sneh and Weinberger, 2003). It  
174 contains well-developed (cm-scale teeth amplitudes) bedding-parallel stylolites, which can be  
175 traced for the full extent of the outcrop, i.e., more than 1km. These are, as far as we know, the  
176 longest measured stylolites reported in the literature. Roughness of these stylolite surfaces was  
177 measured and analyzed by us in a previous paper (Laronne Ben-Itzhak et al., 2012), and is  
178 characterized by a Hurst exponent  $H \sim 0.65$ , and by an upper cutoff for self-affinity at around  
179 50cm. In the lowermost part of the section some interconnected stylolite networks were observed  
180 between the long parallel stylolites.

181 **Mitzpe Ramon Quarry (Fig 2):** In this quarry near the town of Mitzpe Ramon in Southern  
182 Israel, networks of interconnected stylolites appear in massive, subhorizontally stratified,  
183 bioclastic limestone of the Upper Cenomanian Avnon Formation. This site provides 3D  
184 exposures over tens of meters of polished quarry walls. The exposures consist of several vertical  
185 units that differ in stylolites networks' characteristics and in the presence or absence of fractures.  
186 In the unit of focus, where fractures are not common, the stylolites do not terminate *per se*, but  
187 rather connect to each other, so that stylolites can be traced from one side of the outcrop to any  
188 other side. In such networks stylolites delineate ‘islands’ or ‘lenses’ of non-dissolved rock, as  
189 seen in Fig 3 (see site #4 in Supplementary A and in Table 1 for details on other units in this  
190 location).

191 **Umbria–Marche slab, Apennines: (Fig 4):** This is a 3-m-long, 1.2-m-wide and 2-cm-  
192 thick limestone slab of the Calcare Massiccio (CM) Formation (Lower Jurassic) of the Umbria–  
193 Marche of Central Italy. The slab is a wackestone–packstone limestone. The Roughness of the  
194 major stylolites (i.e. a subset of the population, defined below) exposed here was studied by  
195 Karcz and Scholz (2003) and was found to be fractal over 4.5 orders of magnitude (with a Hurst  
196 exponent of  $\sim 0.5$ ). In this site stylolites and veins form various interconnecting geometries.

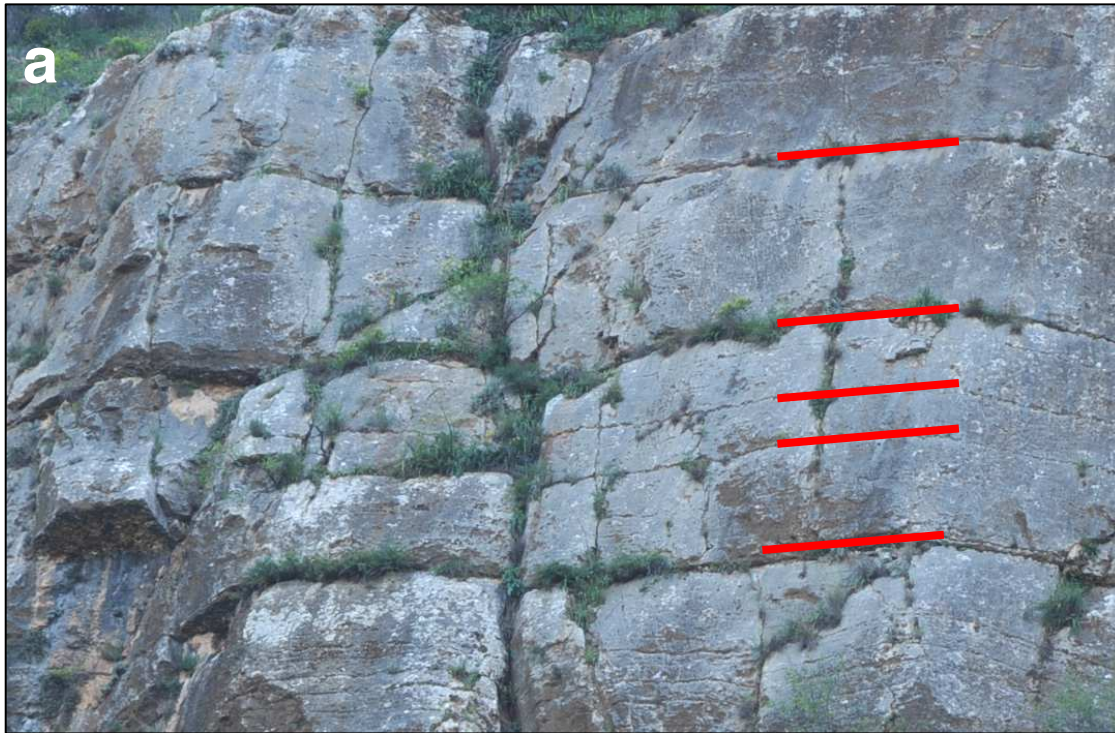


**Fig 1: Long parallel stylolites in the Blanche cliff, Northern Israel.**

**(a) Part of the cliff with four stylolites (labeled '4(19)', '5(7)', '5(9)' and '5(13)' in Figure 5b) marked in red, showing they can be traced for a large distance.**

**(b) Zoom on two other stylolites ('3(10)' marked by a green arrow, and '3(11)', see Figure 5b), where stylolite cm-scale roughness is evident.**



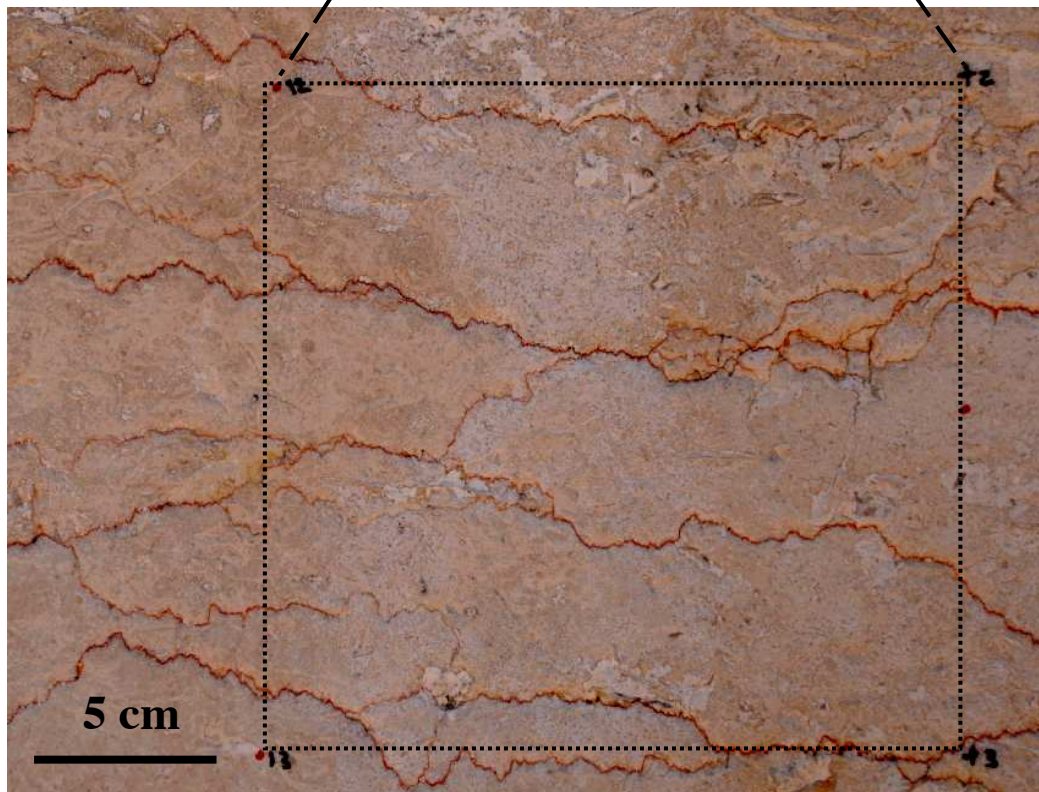
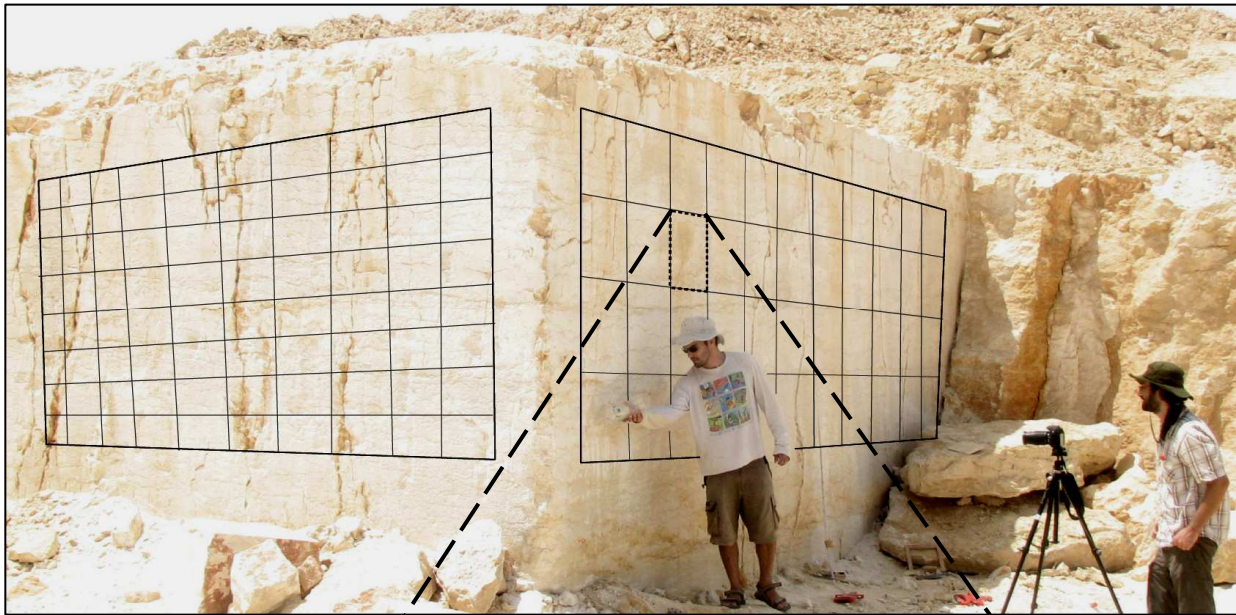


**Fig 2: Interconnected stylolite network (anastomosing) from a Cenomanian limestone quarry near Mitzpe Ramon, Southern Israel.**

**(a) Large scale photo and (b) zoom of the mapped exposure, studied from two perpendicular sides. High-resolution photographs were combined using a grid for digitization of the stylolite network (the black grid in (a) was drawn on the photo to illustrate where the actual grid on the exposure was marked).  $5.5 \times 1.2 \text{ m}^2$  were mapped on either of the two perpendicular sides.**

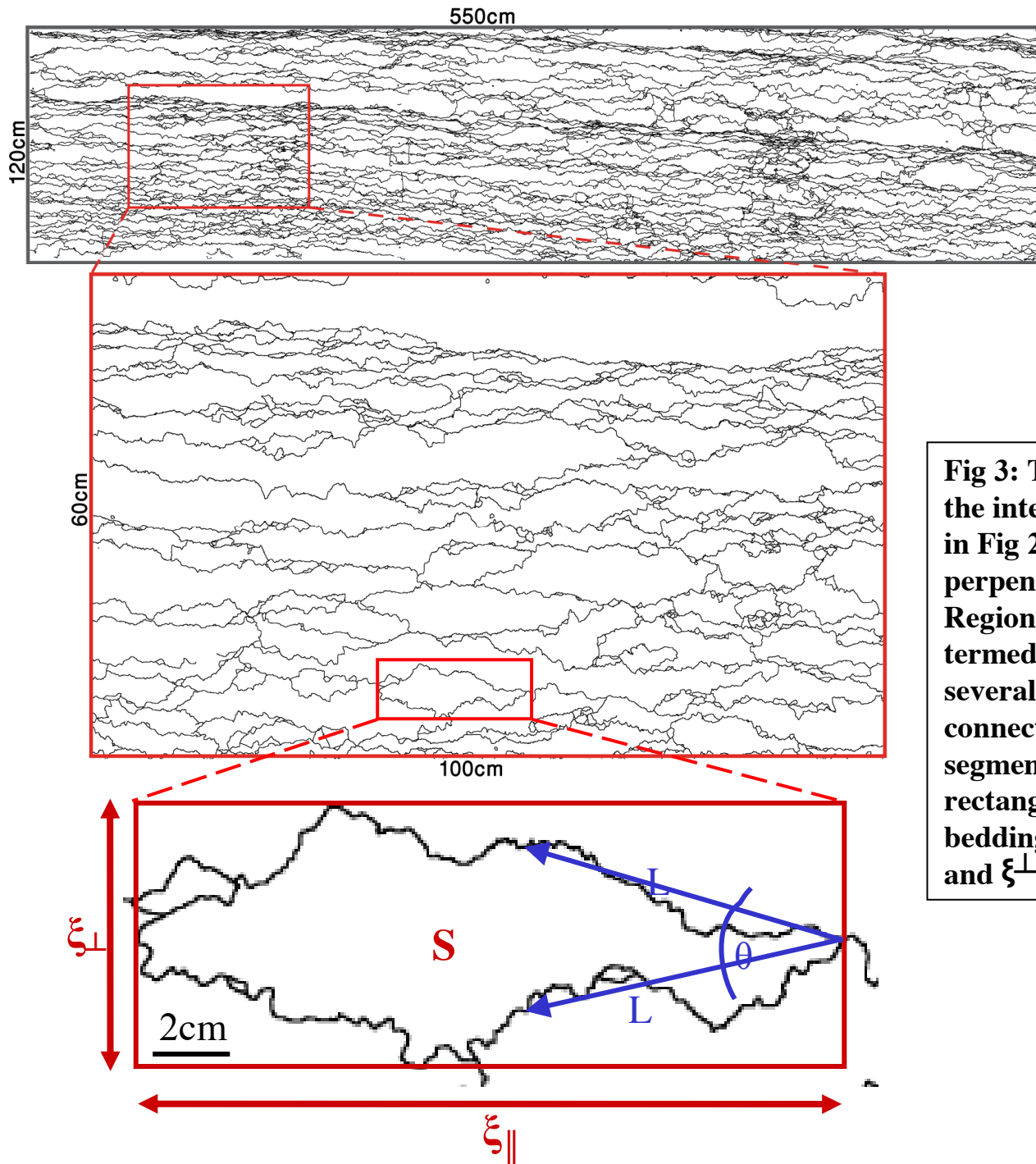
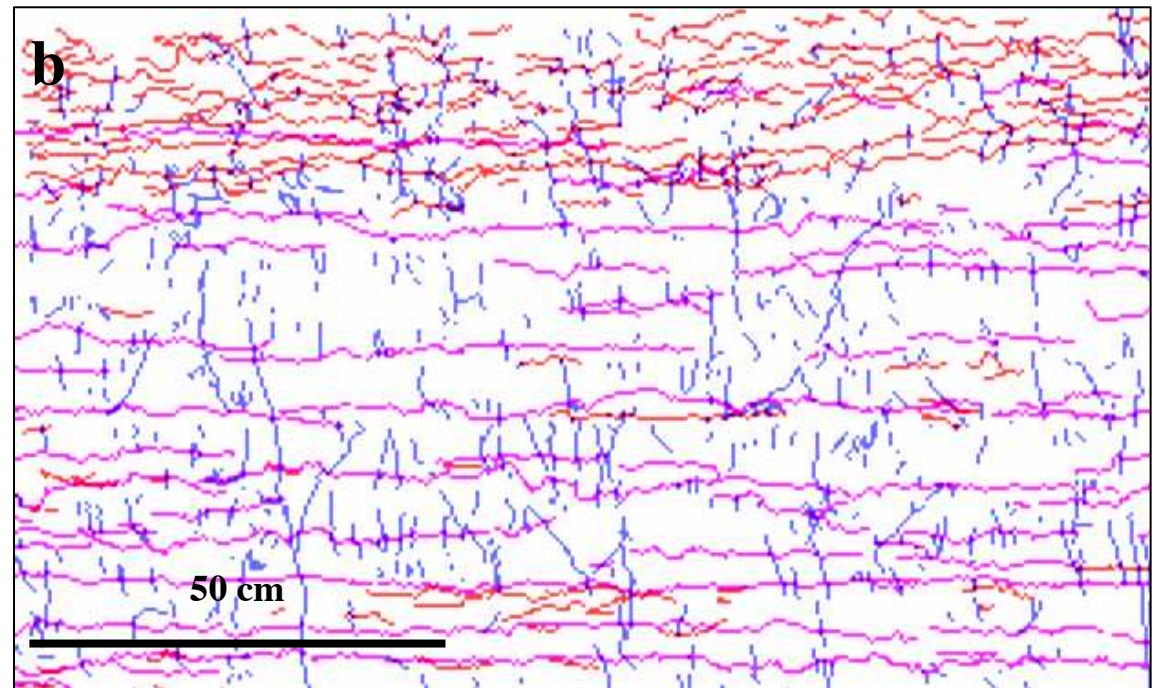


**Fig 3: Three scales of a digitized map of the interconnected stylolite network seen in Fig 2 (the right section of the two perpendicular exposures in fig 2). Regions between connected stylolites, termed “islands”, are described by several parameters: island area  $S$ ; connection angle  $\theta$  between stylolite segments of length  $L$ ; and a bounding rectangle with bedding-parallel and bedding perpendicular dimensions  $\xi_{\parallel}$  and  $\xi_{\perp}$ , respectively.**





Major stylolite    Minor stylolite    Crack

**Fig 4: Interconnected network of stylolites and fractures in limestone (Calcare Massiccio Formation, Jurassic, Italy).**

**(a) photo; and**

**(b) digitized map of major and minor stylolites (pink and red, respectively) and of fractures (blue).**

197

## 198 **2.2 Description of measurements**

199 The type of measurements conducted on the various stylolite populations and their resolution  
200 was tailor-fit to the population characteristics.

201 Long parallel populations –stylolitic roughness was previously analyzed in this cite in order  
202 to study the amount of dissolution on them (Laronne Ben-Itzhak et al., 2012). Here we look at  
203 different characteristics of the same stylolites, namely lateral variations in maximum stylolite  
204 amplitude ( $A_{\max}$ ) and in spacing between them ( $d$ ). These characteristics were chosen in order to  
205 establish uniformity in bedding parallel direction and connectivity in 2D. At the Blanche cliff all  
206 observable stylolites (a total of 65 stylolites) were measured at the northern part of the cliff (Fig  
207 5). The cliff was then divided into 9 units, separated by prominent stylolites. Each stylolite was  
208 named according to its position in the unit (for example: stylolite '3(10)' is the 10th stylolite in  
209 unit 3). Six specific stylolites (‘3(10)’, ‘3(11)’, ‘4(18)’, ‘4(19)’, ‘5(7)’ and ‘5(9)’) that are easily  
210 viewed and are accessible at least in some places along the cliff, were traced and measured in  
211 several stations along the exposure. Spatial measurements were done directly on the cliff using a  
212 tape, or, where access was difficult, on digital images. Since stylolites are fractal surfaces (Karcz  
213 and Scholz, 2003, Renard et al., 2004, Schmittbuhl et al., 2004, Ebner et al., 2009b), properties  
214 such as mean and maximum amplitude depend on the scale of observation,  $l$ . Therefore  $A_{\max}$  was  
215 defined here as the maximum distance from peak to crest along  $l=1\text{m}$  length (based on Laronne  
216 Ben-Itzhak et al. (2012)).

217

218 Anastomosing networks In this type of population islands of rock are captured and become  
219 isolated between stylolites, while stylolites meet, join, and percolate in all directions. Such  
220 systems are somewhat more complex to characterize than long parallel stylolites. For example,  
221 both stylolite amplitudes and spacing are ill-defined in anastomosing networks. We thus chose to

222 characterize such networks via (as defined in Fig 3): a) connection angle ( $\theta$ ) between stylolites  
223 and b) the dimensions of “islands” demarcated by stylolites. At the Mitzpe Ramon site, the 10m  
224 columnar section was studied at several locations in the quarry and was then divided into 5 units,  
225 characterized by different density of the stylolite network, different fossils, and presence or  
226 absence of fractures (Kaduri (2013), and see also supplementary A). We chose to focus on one of  
227 these units, in which fractures and veins are rare and which does not contain large fossils. To  
228 obtain connection angle and island dimensions for the entire network, the stylolites in this unit  
229 were digitized from digital images (200 $\mu$ m resolution) to yield two perpendicular maps (550x120  
230 cm each, Fig 3). The digital maps were then saved as grids composed of squares colored black  
231 for stylolites or white for rock (Fig 3c). The black and white maps were analyzed using image-  
232 processing tools in MatLAB and MatLAB codes written in Kaduri (2013) to obtain:

- 233 1. Values of connection angle  $\theta$  measured between each two connecting stylolite lines, as a  
234 function of the distance  $L$  from their meeting junction, as defined in Fig 3.
- 235 2. In order to obtain island dimensions, regions between stylolites (“islands”) were digitally  
236 identified, and each of the islands given a serial number. In this way more than 3000 islands were  
237 obtained. Each island was then bound by a rectangular box (a “bounding box”), with horizontal  
238 and vertical lengths  $\xi_{\parallel}$  and  $\xi_{\perp}$ , respectively (as depicted in Fig 3), to provide an estimate of their  
239 lateral and vertical dimensions. The scaling behavior of the networks may be partially revealed  
240 by studying the dependence between  $\xi_{\parallel}$  and  $\xi_{\perp}$  for each island. Similar analysis was performed  
241 on fluid cluster populations in two-phase flow in porous media (Tallakstad et al., 2009a,  
242 Tallakstad et al., 2009b) and on networks of propagating fracture fronts, to extract the statistics  
243 of rupture avalanches (Maloy et al., 2005, Maloy et al., 2006, Tallakstad et al., 2011).

244

245 *Stylolite-fracture networks.* The stylolites and fractures in the network of the third site were  
246 digitized on the slab at a 0.5mm resolution. This type of network is composed of long, sub-  
247 parallel stylolites, which extend from one side of the slab to the other (termed here “major”



248 stylolites), and shorter (defined here as “minor”) still sub-parallel, stylolites (Fig 4b). In addition  
249 the network is composed also of fractures that illustrate geometrical interactions with stylolites,  
250 as shown below. Orientations of stylolites and of fractures were studied statistically, and  
251 qualitative descriptions of interactions between fractures and stylolites were made, in order to  
252 constrain the mechanical evolution of this network and its associated strain.

253

### 254 **3. Results and data analysis**

255

256 The measurements conducted in the three key field-sites are presented here by site.

257

#### 258 **3.1 Long-parallel stylolites in the Blanche cliff**

259 A crucial finding in the Blanche cliff site (and in sites #5, 6, 7, 11 and 12 shown in the  
260 Supplementary Material) is that most stylolites are as long as the ~1km outcrop and are parallel  
261 to each other and to the bedding. No fractures or joints related to the stylolites were observed and  
262 the major faults, which terminate the exposure on both sides, are post-stylolitization. Two  
263 variables were measured along the cliff exposure to detect spatial variations: spacing between  
264 adjacent stylolites ( $d$ , defined in Fig 5), and maximum teeth height of individual stylolites ( $A_{\max}$ ).  
265 Although  $d$  ranges from 0.1 to 2.0 meters when looking at different neighbors, the spacing  
266 between any two given stylolites is laterally constant, as seen qualitatively in Fig 1 and as  
267 quantitatively measured over ~1km in Fig 6a. For example,  $d$  between stylolites 3(10) and 3(11)  
268 varies (without any obvious spatial trend) between 15 and 22 cm along 850m of the exposure.

269 The lateral variation of maximum stylolite amplitude ( $A_{\max}$ ) in the Blanche cliff shows no  
270 particular trend, i.e. it does not decrease or increase gradually in any direction (Figs 6b, 6c). For  
271 example,  $A_{\max}$  of stylolite 3(10) varies between 2.5 and 5.5 cm, which in itself may be  
272 significant, but does not vary consistently in any direction (e.g. from the center of the cliff

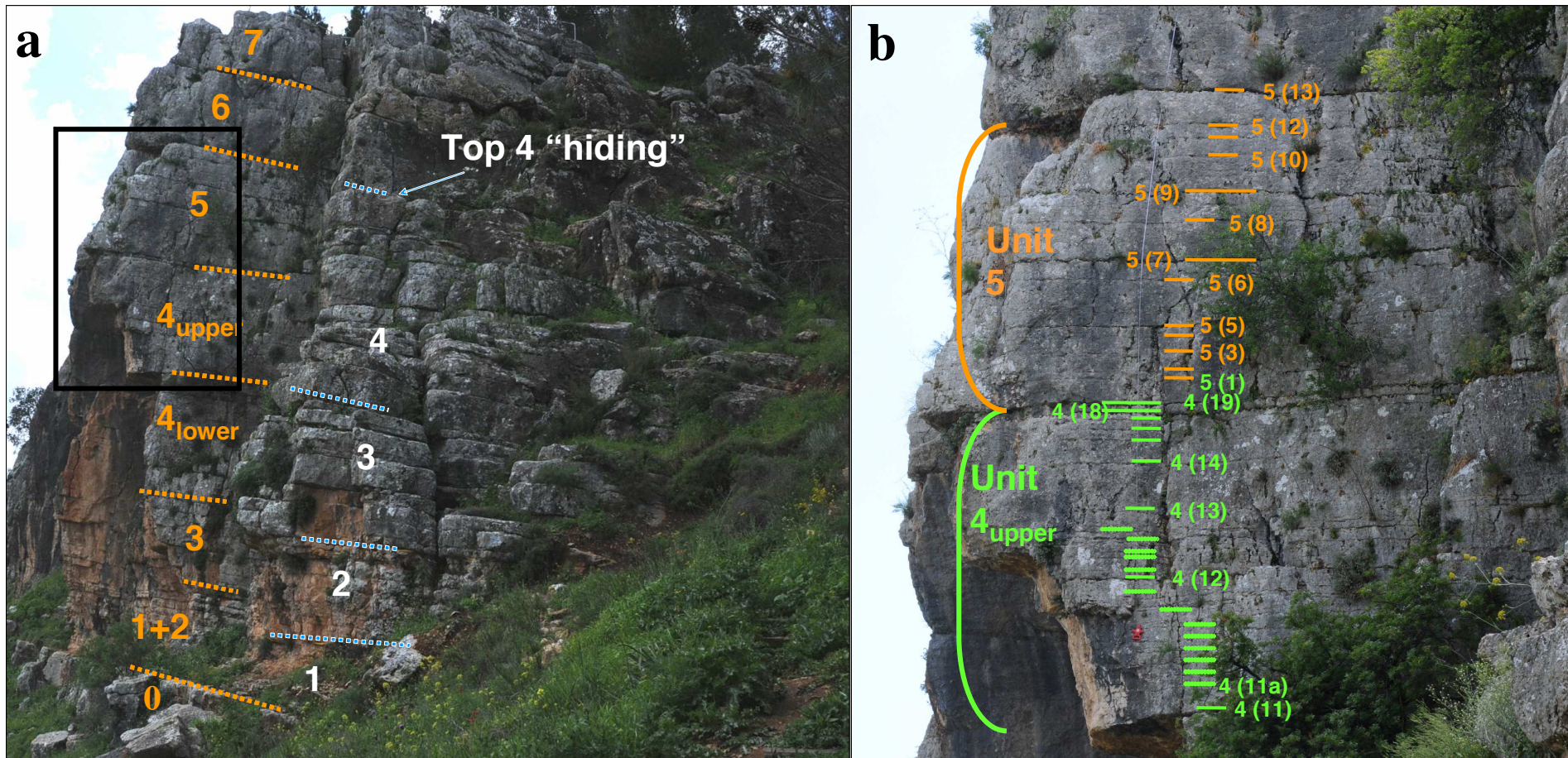


**Fig 5: Images showing the Blanche (Ein El-Assad Fm.) section in the northern part of the cliff, where all 65 stylolites were identified and measured.**

**(a) The section was divided to 9 major units differentiated by major stylolites (in orange). Most of the measurements were performed in the parts that are marked in white, which are more accessible.**

**(b) Zoom on rectangle in (a). Stylolites are labeled according to their vertical position within a unit, i.e., 5 (3) is the third stylolite from the bottom of unit 5.**

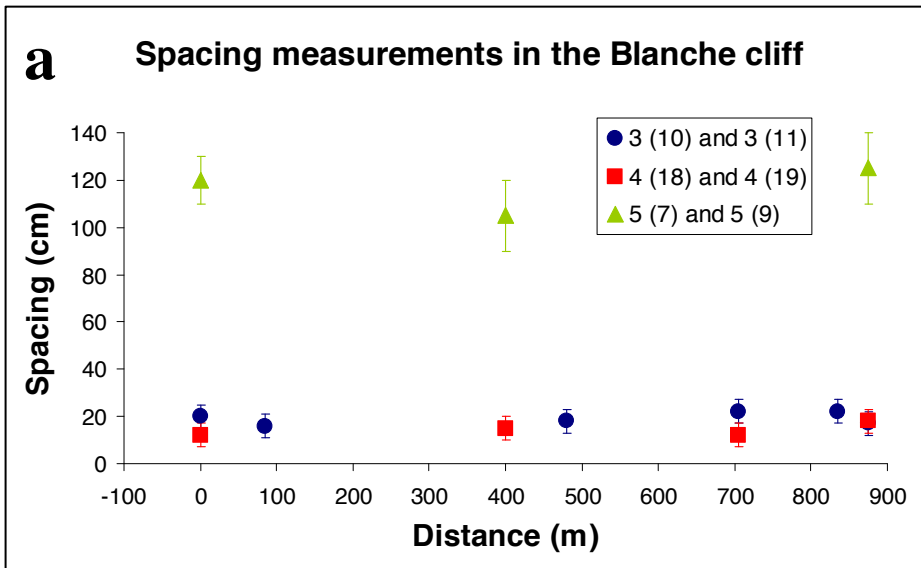
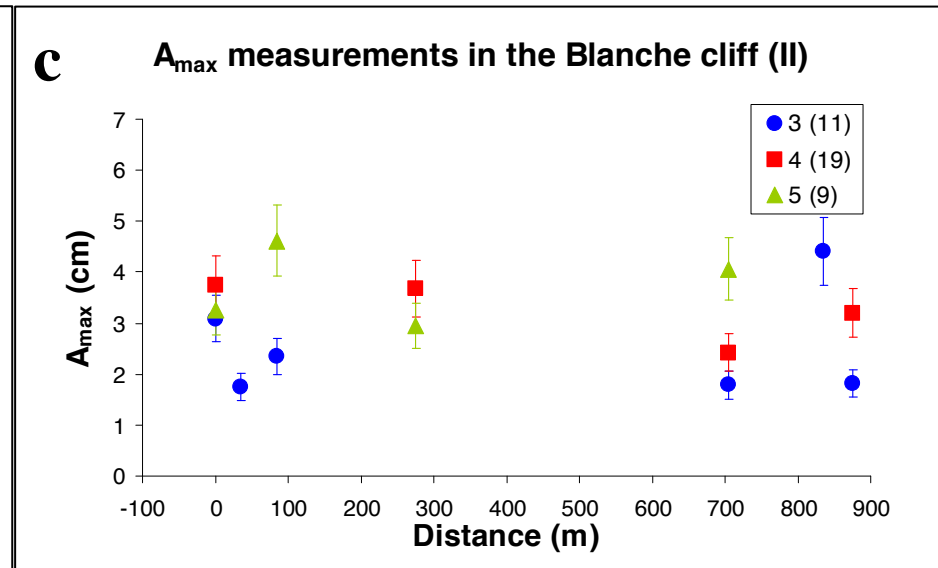
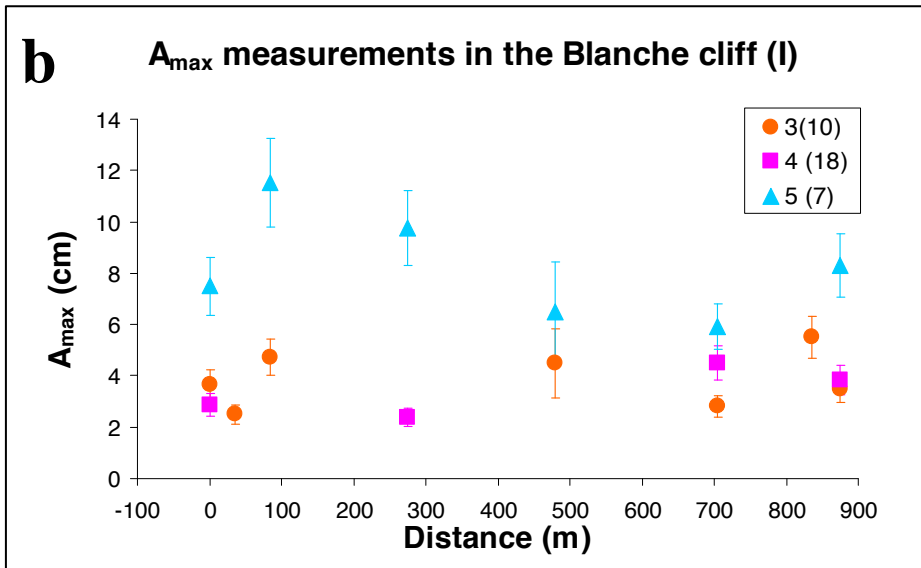


**Fig 6: Measurements conducted on long parallel stylolites at several locations along the ~1km – long Blanche cliff.**

**(a) Spacing between three couples of stylolites.**

**(b) and (c) Maximum teeth amplitude ( $A_{max}$ ) of six different stylolites (viewed in two separate graphs only for purposes of convenience). Error bars are the standard deviation of several measurements in each location. No trend in spacing or  $A_{max}$  along the length of the stylolites is identified.**



273 sideways, or from one end to the other). This either suggests that terminations are still far away,  
274 or that the observations and conclusions of Mardon (1988) and Stockdale (1922) on isolated  
275 seams, showing tapering of seam thickness and teeth amplitude from center to edges, do not  
276 apply here. This will be discussed below.

277

### 278 **3.2 Anastomosing stylolite network in Mitzpe Ramon Quarry**

279 We focus here on statistics of islands formed by stylolites. The islands vary widely in size,  
280 from centimeter to a couple of meters in width and length, yet show robust characteristics: Fig 7a  
281 shows the connection angle,  $\theta$ , between two connecting stylolites, as a function of the distance  
282 from their junction,  $L$ , as defined in Fig 3. Each data point is the average of all  $\theta(L_i)$  in the  
283 exposure and the error bars are the standard deviation, both produced from normal distribution  
284 best-fits to each value of  $L$  (inset in Fig 7a). Connection angle in the anastomosing stylolite  
285 network of the Mitzpe Ramon Quarry is found to be distance dependent. Close to the connection  
286 points, i.e. for  $L < 2\text{cm}$ ,  $\theta = 80^\circ - 90^\circ$ , but this value decreases asymptotically to zero (stylolites  
287 become sub-parallel) for larger values of  $L$ . This means that stylolites meet at near perpendicular  
288 angles (similarly to cracks), but approach parallel planes when far “enough” apart ( $L \gg 5\text{cm}$ ).

289 Fig 7b shows vertical versus horizontal dimensions ( $\xi_{\perp}$  versus  $\xi_{\parallel}$ ), of over 3300 islands  
290 analyzed in this site. We identify a robust power-law relation between the height and width of  
291 islands: Performing a linear fit in bi-logarithmic space of  $\xi_{\perp}$  versus  $\xi_{\parallel}$ , we obtain

$$292 \quad (1) \quad \xi_{\perp} = k \xi_{\parallel}^{\alpha}$$

293 with  $k [m^{1-\alpha}] = 0.67 \pm 0.01$  and  $\alpha$  (unitless) =  $0.67 \pm 0.03$  (The reason that both constants are  
294 equal is probably by chance).

295

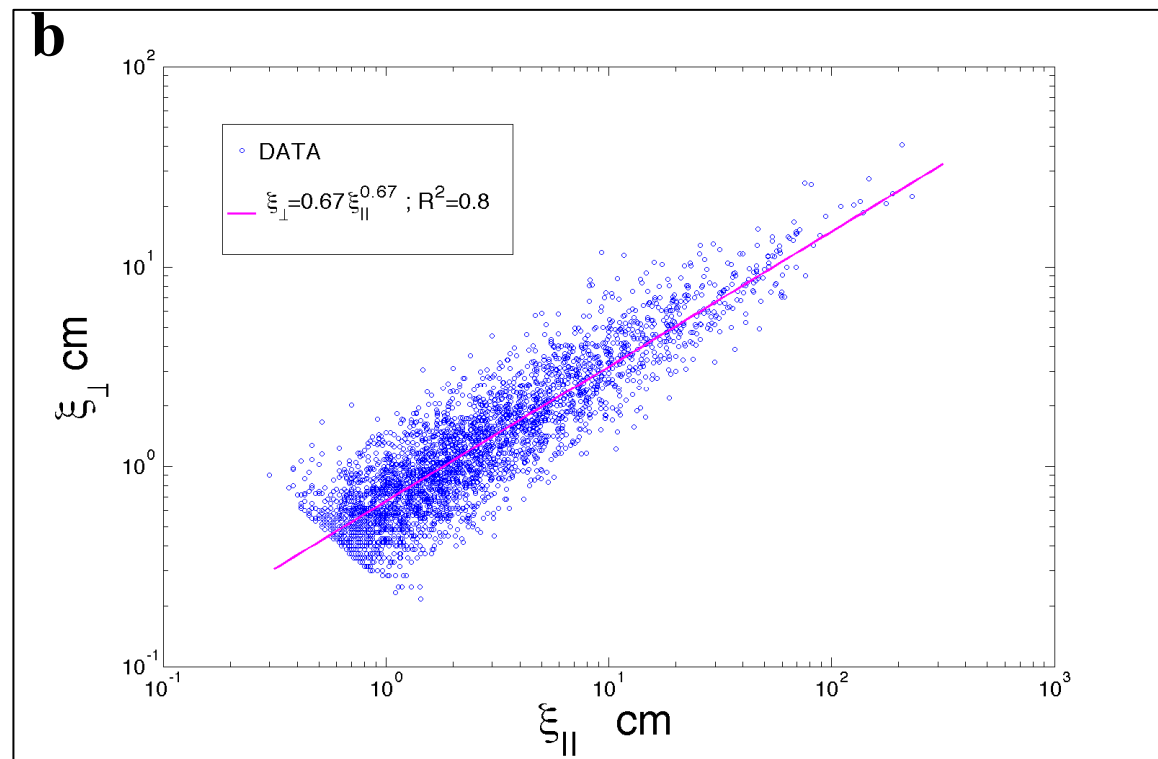
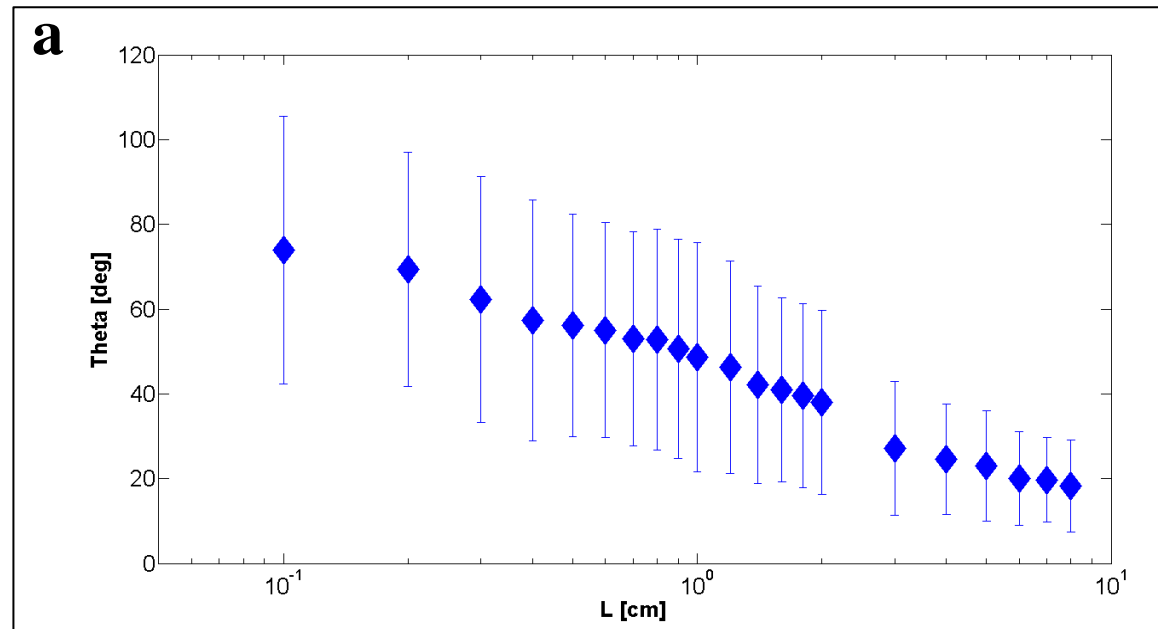
**Fig 7:**  
**Results of the statistical analysis**  
**performed in Mitzpe Ramon quarry.**

**(a)  $\theta(L)$  and**

**(b) Island dimensions, as explained in**  
**the text.**

**The variables are illustrated in Fig 3c.**  
**Each data point in (a) is the average of**  
**all  $\theta(L_i)$  in the exposure and the error**  
**bars are the standard deviation.**

**The pink line in (b) is a best fit to the**  
**correlation between  $\xi_{\perp}$  and  $\xi_{\parallel}$  with**  
**both  $a$  and  $k$  equal 0.67.**



296 **3.3 Stylolite-fracture network in the *Umbria–Marche* slab, Apennines**

297 We view the major stylolites of this slab (Fig 4b) as a long-parallel population (shown to be  
298 fractal over 4.5 orders of magnitude (Karcz and Scholz, 2003)), whereas the minor ones are  
299 either anastomosing, connected to fractures, or isolated. Many of the fractures have clear  
300 interactions with the stylolites, e.g. emanating from-, or connecting between- stylolite tips, or  
301 emanating from stylolite teeth. Stylolites and fractures are found to be generally perpendicular to  
302 each other, as seen qualitatively in Fig 4b and quantitatively in Fig 8. However, a significant  
303 population of fractures that are sub-parallel to the stylolites is also seen in Fig 8.

304

305 ***Small-scale observations***

306 Relations between stylolites and fractures in this network imply that the two types of  
307 features are probably related to one another (Fig 9). Stylolites are often connected to each other  
308 via fractures (Figs 9a, 9d, and 9f), though regions of anastomosing stylolites are also quite  
309 common (Fig 9c). Fractures in this network are either Mode I veins or Mode II shear fractures  
310 with some offset. Fractures interpreted as Mode II shear fractures based on geometrical  
311 considerations, may exhibit small “pull-apart” features filled with cement (Fig 9a). Many Mode I  
312 veins appear at some acute angle to stylolites while others emanate from stylolite teeth (or what  
313 seem to be terminations) and are perpendicular to the stylolite mean surface (Fig 9b). Veins  
314 connected to stylolites often taper away from the stylolite (e.g. Fig 9b). Similar tapering was also  
315 described by Eren (2005). Some fractures simply connect neighboring stylolites (Figs 9a, 9f)  
316 while complex connections, such as in Fig 9d, are very common as well. At the scale of  
317 observation, some features appear not to be fully physically connected (e.g. Figs 9b, 9d). Perhaps  
318 there is connection in 3D that is not seen in the 2D view. Even when the connections are more  
319 difficult to observe, such as in Fig 9b, geometry suggests strain-related interactions between the  
320 stylolites and fractures.



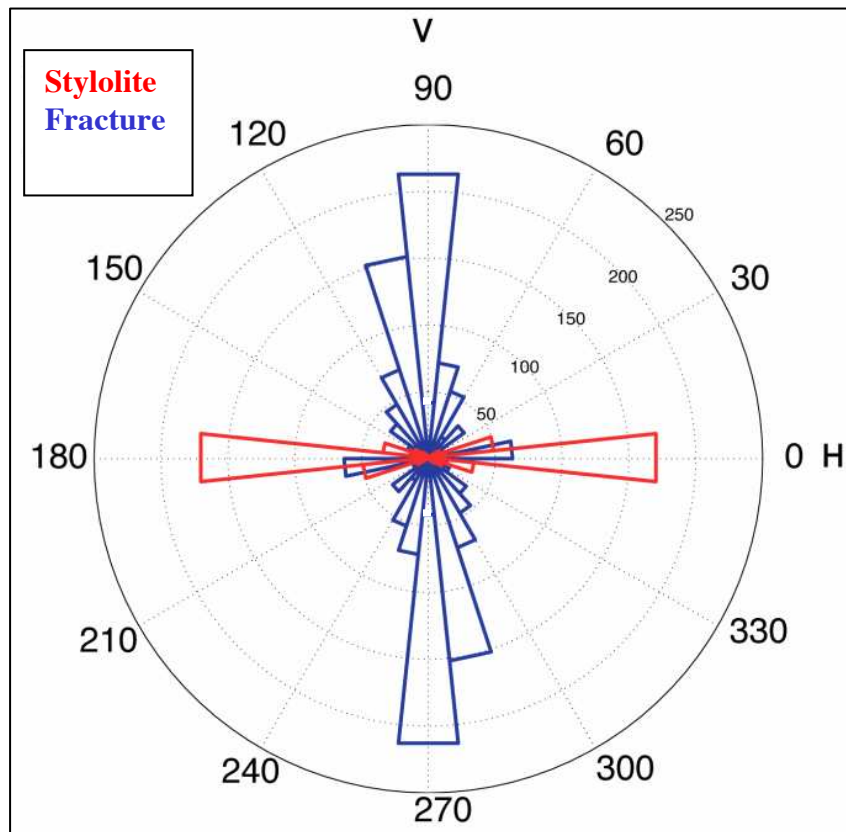


**Fig 8: Orientations of stylolites and fractures in the Umbria–Marche slab, Apennines (analyzed upon map in Fig 4).**

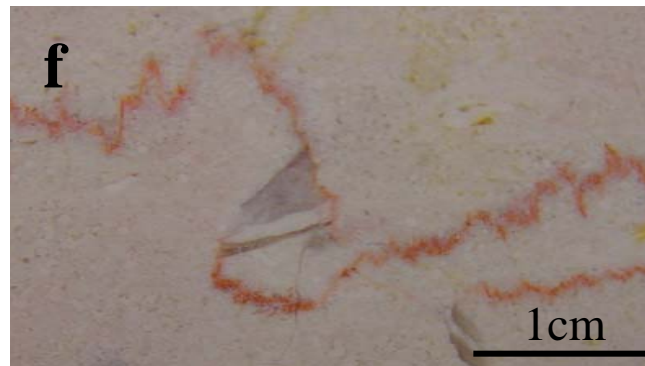
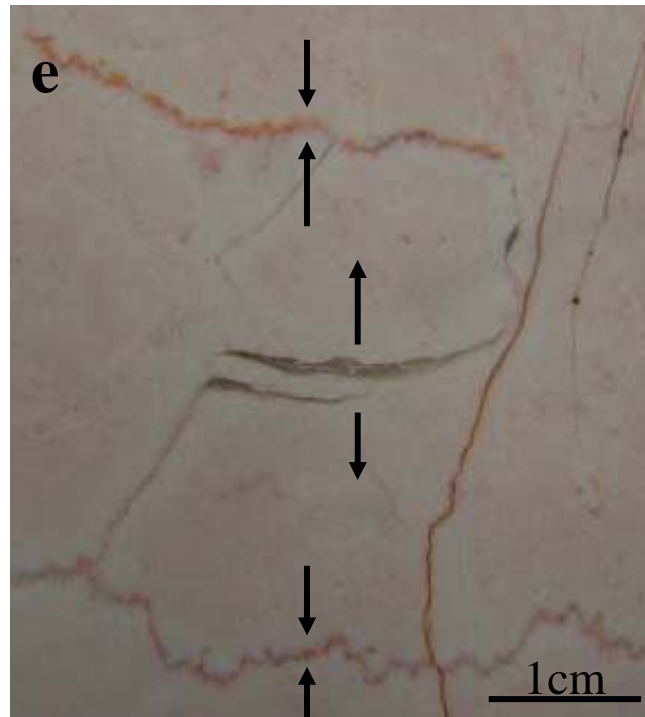
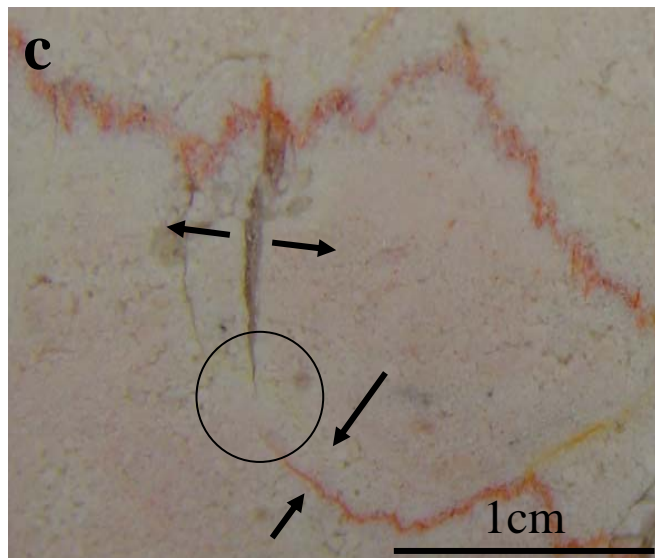
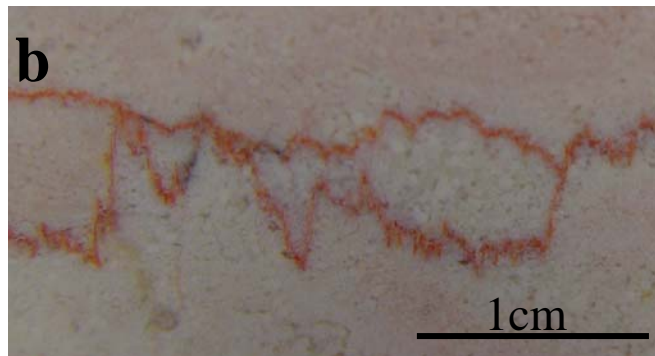
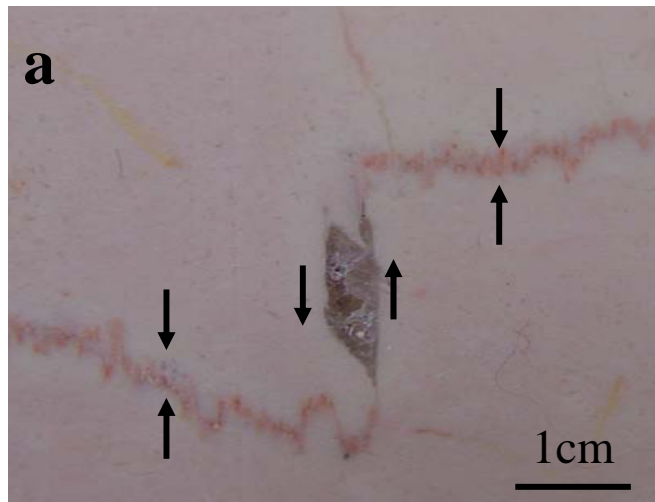


**Fig 9: Zoom-in on the slab of Fig 4 showing small-scale field-relations between fractures and stylolites and between the stylolites themselves.**

**(a) Mode II fracture with pull-apart structure filled with cement connecting two stylolites. Interpreted strain direction is marked by arrows.**

**(b) Interconnected stylolite network that seems to be derived from stylolite "cannibalism" (see text for further explanation).**

**(c) Mode 1 veins sub-parallel to the stylolite teeth and splaying from them. The veins are commonly triangular, with the aperture being largest close to the stylolite surface. stylolite mean direction is changed near a vein (circled region).**

**(d) Complex connection between non-overlapping stylolites by an array of oblique veins.**

**(e) Veins parallel to stylolite surface mean direction indicating on extension that is in the same direction as compression (see arrows). This population of fractures parallel to stylolites is statistically common (see Fig 8).**

**(f) Vein and stylolites closely interacting. We interpret such intimate geometries as indicating on these features to be syn-formational.**

**Figs 9a, 9b and 9c illustrate possible mechanisms for the formation of the observations in Figs 8a, 8b and 8c, respectively.**



321 Veins parallel to the mean surface of the stylolite are seen in Figs 9e, and are statistically  
322 important (Fig 8). Explanations and implications of this observation are suggested in the  
323 discussion.

324

325

## 326 **4. Discussion**

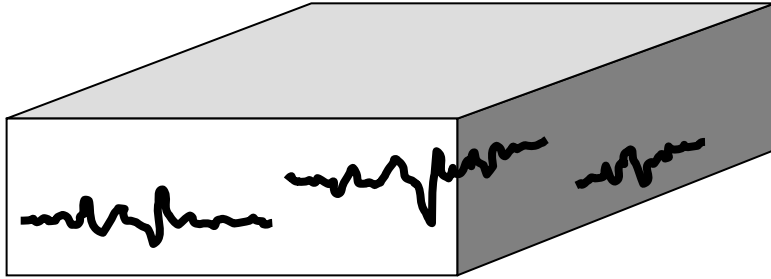
327 We suggest using natural divisions provided by percolation theory, in order to  
328 characterize the connectivity of natural stylolite populations. Pervious classification schemes for  
329 stylolites and pressure solution addressed roughness, spacing, relation to bedding and seam  
330 geometry (Park and Schot, 1968, Alvarez et al., 1978, Powell, 1979, Guzzetta, 1984, Engelder  
331 and Marshak, 1985, Railsback, 1993). Although these are very useful quantification approaches  
332 for classifying single stylolites, they do not address quantification needs for describing  
333 connectivity, as percolation theory offers.

334 Based on the observations and measurements presented above and on the theoretical  
335 possibilities for connectivity/percolation of surfaces in a 3-D space (presented in the  
336 introduction), we may categorize sedimentary stylolite populations into three  
337 connection/percolation geometries (Fig 10):

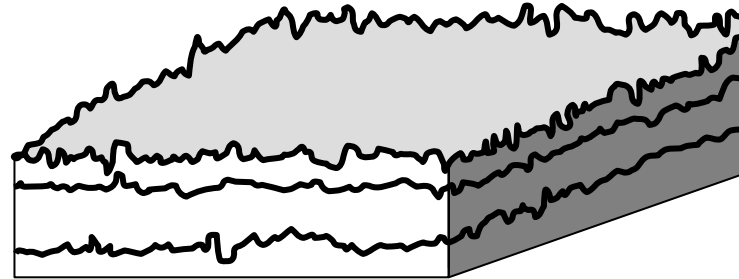
### 338 **Class I: Isolated stylolite populations - no percolation of stylolites (Fig 10a):**

339 These are stylolitic surfaces with clear terminations and no connections to other stylolites  
340 or fractures. Stockdale (1922) and Mardon (1988) report finding isolated stylolites and solution  
341 seams, respectively, in carbonates. Benedicto and Schultz (2010) investigated isolated tectonic  
342 stylolites and the strain associated with them in a ~0.2m-thick limestone layer in a fault-damage  
343 zone. Nenna and Aydin (2011) describe isolated tectonic solution seams in a sandstone  
344 formation.

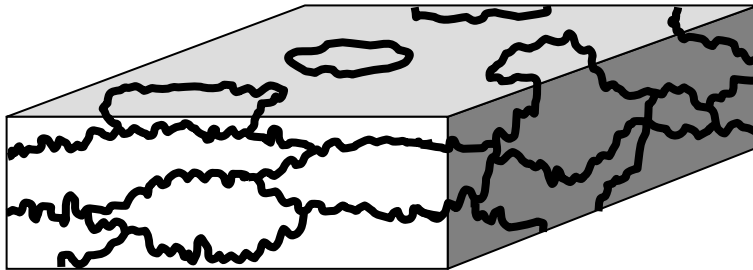
a) Isolated stylolites (*zero connectivity*)



b) Long bedding-parallel stylolites (*2D connectivity*)



c1) Anastomosing stylolite network (*3D connectivity*)



c2) Stylolite-fracture network (*3D connectivity*)

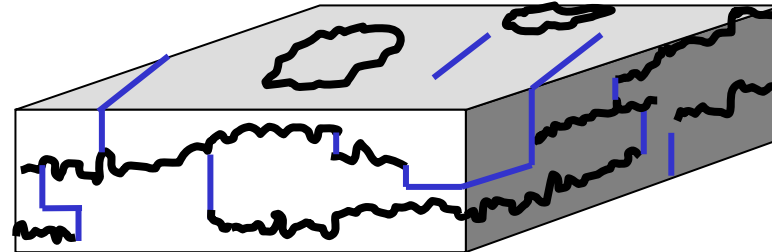


**Fig 10. Connectivity-based classification of sedimentary stylolite populations: (a) Isolated stylolites; (b) Long bedding-parallel stylolite population; and (c) Interconnected-network stylolite population, further divided into (c1) anastomosing networks of stylolites and (c2) interconnected networks of stylolites and fractures (fractures appear in blue).**

345 **Class II: Long, bedding- parallel, stylolite populations - 2D percolation of stylolites**

346 **(Fig 10b):**

347 In this group stylolites are virtually infinite bedding-parallel rough surfaces that do not  
348 connect since they are parallel. These stylolitic surfaces have roughness with amplitude smaller  
349 than the spacing between them, so they also don't overlap. Tracing these surfaces connects the  
350 rock body from side-to side in 2 dimensions, sub-parallel to bedding, but not in the 3<sup>rd</sup>  
351 dimension, perpendicular to the surfaces and to bedding. Long bedding-parallel stylolites (or  
352 solution seams) were seldom described in the literature (Park and Schot, 1968, Safaricz, 2002,  
353 Safaricz and Davison, 2005).

354 **Class III: Interconnected stylolite networks- 3D connectivity (Fig 10c):**

355 Here stylolite surfaces are connected to one another by anastomosing or via fractures and  
356 veins. One can trace along these surfaces, following a "stylolite pathway", from any side of the  
357 rock to any other side, since surfaces percolate in 3 dimensions. Interconnected stylolite  
358 networks can be further divided into *anastomosing stylolite networks* and *stylolite-fracture*  
359 *networks*. Interconnected stylolites were reported in several references (Mardon, 1988, Rye and  
360 Bradbury, 1988, Peacock and Sanderson, 1995, Smith, 2000, Safaricz, 2002, Eren, 2005).

361

362 The stylolite populations in our investigated sites either clearly fall into one of the 3 end-  
363 member connectivity classes, or present a combination of more than one class. *Long, parallel*  
364 *stylolite populations* (Fig 10b) and *Interconnected networks* (Fig 10c) are both commonly  
365 observed in field locations, as seen in the Supplementary Material (sites # 4-16). *Isolated*  
366 *stylolites* (Fig 10a) were not observed as a separate class in our field sites. Several stylolites in  
367 the stylolite-fracture network in the Umbria-Marche slab seem to terminate in our observed 2D  
368 plane, but possibly they are connected in 3D. The last site reported in the Supplementary (#17) is  
369 the only location with isolated features (often forming networks) and for this reason we included  
370 it, although the features are solution seams and not stylolites. Based on our fieldwork and on

371 literature, it appears that isolated stylolites are uncommon, though isolated pressure solution  
372 seams are not rare (Mardon, 1988, Nenna and Aydin, 2011). In terms of evolution, isolated  
373 stylolites, the non-percolating structure, may only be an intermediate stage in the evolution  
374 process of percolating stylolites (which might explain their scarcity), as discussed in the next  
375 sub-section. But in terms of topology isolated stylolites are one of the 3 topological possibilities  
376 for connectivity of stylolitic planes, so for the sake of characterizing morphology we propose to  
377 consider them as a separate class – the class of “no connectivity”.

378 The Supplementary Material presents 14 additional field sites with large-scale stylolite  
379 exposures. Out of these, 3 have long-parallel stylolite populations, 6 have interconnected  
380 networks of both sub-groups, while 4 sites present a combination of end-member connectivities.  
381 Combinations were mostly of long parallel stylolites with anastomosing network in between.

382

#### 383 ***4.1 Conceptual model for formation of observed stylolite populations***

384 Here we present a conceptual model of stylolite population formation to facilitate an  
385 understanding of strain accommodation by stylolite populations. We review briefly the formation  
386 of isolated and long-parallel stylolites, as it is discussed and modeled in detail in Aharonov and  
387 Katsman (2009) and Laronne Ben-Itzhak et al. (2012), respectively. Table 2 summarizes how our  
388 field measurements support suggested formation mechanisms for each of the different  
389 populations.

390

##### 391 **4.1.1. Isolated stylolites:**

392 The amount of discussion of the formation of this type of population (Fletcher and Pollard,  
393 1981, Mardon, 1988, Aharonov and Katsman, 2009) is inversely proportional to their prevalence.  
394 These constitute Localized Volume Reduction (LVR) defects, as defined by Katsman and  
395 Aharonov (2005), and Katsman et al. (2006a, b). Field observations of these features show

**Table 2:** Summary Table: suggested mechanisms for evolution of the various stylolite populations and the type of measurements that support each mechanism

Population Type	Suggested Mechanisms	Measurements	How Measurement Supports Mechanism
Isolated stylolites; zero connectivity	Initiation from seed, continuing dissolution and elongation due to both stress and composition (clay?)	$A_{max}$ versus Length	If more developed (large $A_{max}$ ) in center and less towards edges, may indicate in-plane-propagation.
Long-Parallel stylolites; 2D connectivity	Initiation and continuation of roughening and dissolution on an existing surface (of higher clay content?)	- $A_{max}$ versus Length -Spacing versus length - Surface roughness	Constant $A_{max}$ , constant spacing between stylolite pairs along the surface, and upper cutoff to self-affinity suggest roughening of an existing surface.
Anastomosing stylolite networks; 3D connectivity	Cannibalism of bedding-parallel stylolites  AND/OR  Joining of isolated stylolites	-Intersection angle         -Island dimensions	Finding of intersection angle of 35°-45° may support formation by joining of isolated stylolites; If angle is random – supports cannibalism. If around 90°, supports connection by fractures  Understanding how to use the statistical characteristics of Islands to estimate the amount of dissolution, depends on the physics of network formation (discussed in the text)
Stylolite-fracture network; 3D connectivity	Increased shear-stress near stylolite tips  AND/OR  Connection of stylolite tips with Mode I cracks	-Directions (angles of stylolites and of fractures) -Small-scale field relations	Pull-aparts adjacent to stylolite tips  Mode I cracks seem to attract stylolite tips.

### **References which appear in Table 1**

1. Safaricz, M., *Pressure solution in chalk*. 2002, Royal Holloway University of London.
2. Arzani, N., *Stylolite networks in dolomitized limestones and their control on polished decorative stones: a case study from the Upper Cretaceous Khur quarries, central Iran*. *JGeope*, 2011. **1**(2): p. 25-37.
3. Losonsky, G., *Burial depth and lithofacies control of stylolite development in the Mississippian Salem Limestone, Illinois Basin*. 1992, University of Cincinnati.
4. Mardon, D., *Localized pressure solution and the formation of discrete solution seams*. 1988, Texas A&M University.

396 geometrical characteristics similar to cracks: (1) their amplitude and thickness taper towards their  
397 edges and (2) their length increases with increasing seam thickness and amplitude (Stockdale,  
398 1922, Mardon, 1988). Such features may develop self-similarly from an initial seed defect,  
399 provided that it grows laterally sub-parallel to its plane and experiences continued dissolution on  
400 its flanks (e.g. Fletcher and Pollard (1981)). Aharonov and Katsman (2009) show that  
401 development of isolated stylolites can be explained by a feedback that arises when both clay  
402 (present in the rock at some small fraction, and in initially higher content in seed defects) and  
403 pressure solution enhance the dissolution process. Nenna and Aydin (2011) suggest that they  
404 elongate and thicken due to the presence of asperities.

405

406 **4.1.2. Long, parallel stylolite populations:** The formation of this abundant, yet rarely  
407 acknowledged, population type was indirectly studied before: the group of Ebner and Kohen  
408 (Renard et al., 2004, Schmittbuhl et al., 2004, Koehn et al., 2007, Ebner et al., 2009a, Ebner et  
409 al., 2009b) studied roughening from a prescribed surface. We suggest long parallel stylolites  
410 form on planes where dissolution is for some reason enhanced, possibly due to initial chemical  
411 heterogeneity (e.g. higher initial content of clay or other dissolution enhancing chemical  
412 heterogeneity). In sedimentary stylolites such planes are most commonly bedding planes. Our  
413 conceptual model suggests that long parallel stylolites do not evolve by lateral elongation of  
414 isolated stylolites, but instead by dissolution-roughening on a preexisting plane, as suggested in  
415 Laronne Ben-Itzhak et al. (2012). This is implied by the constant roughness amplitude we  
416 measured along almost 1km (Fig 6), which does not follow the observed „parabolic’ self-similar  
417 profile of dissolution along isolated stylolites (Stockdale, 1922, Mardon, 1988). In  
418 supplementary B we present a simple calculation that shows that the amount of dissolution on the  
419 Blanche stylolites would have been far larger than measured if they evolved by elongation from a  
420 seed rather than roughening of an existing surface. Spatially constant amplitude, as observed  
421 here, is consistent with a process invariant under translation along the stylolite. It is easiest to

422 explain the observed long parallel stylolites as forming by localized dissolution on an initially  
423 flat plane (most often a bedding plane), that progressively roughens with time, driven by  
424 competing effects of stress, diffusion and noise (Koehn et al., 2012, Laronne Ben-Itzhak et al.,  
425 2012, Rolland et al., 2012). The dissolution creates a self-affine surface, following a scaling law  
426 between the out-of-plane root mean square width,  $w(l)$ , and the in-plane length,  $l$ , at which this  
427 width is defined:  $w(l) \sim l^H$ , with a Hurst exponent  $H \sim 0.65$ , and with an upper cutoff for self-  
428 affinity that grows with increasing amount of dissolution (Renard et al., 2004, Schmittbuhl et al.,  
429 2004, Koehn et al., 2007, Ebner et al., 2009a, Laronne Ben-Itzhak et al., 2012).

430

#### 431 **4.1.3. Interconnected stylolite networks**

432 This is again a very common type of population (sites # 2-6, 8-10, 13-16), which has not  
433 received much previous attention, and its formation has rarely been discussed. Based on our  
434 field observations, we propose that interconnected networks can form by one of three  
435 mechanisms or through a combination thereof. The three mechanisms are: (i) *Connection of tips*  
436 *of isolated stylolites* via dissolution or Mode II fractures; (ii) *Connection of stylolite tips with*  
437 *Mode I cracks* (iii) *Connection of long parallel stylolites*; (Figs 11a, 11b and 11c, respectively,  
438 linked to the examples in Figs 9a, 9b and 9c, respectively). In (i) and (ii) a population of non-  
439 touching surfaces of type (a) in Fig 10, connects as it evolves to finally create a percolating  
440 structure. In (iii) initially sub-parallel planes (type b in Fig 10) roughen enough with time to  
441 connect in the bedding perpendicular direction.

442

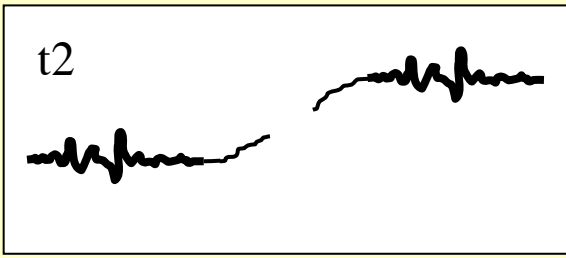
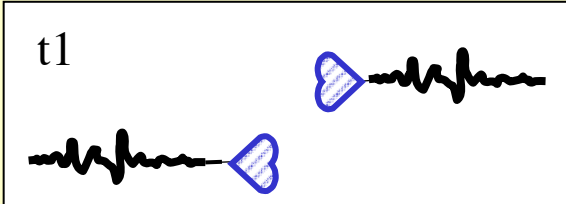
443 **(i) Connection of tips of isolated stylolites**: This may occur when two neighboring LVRs  
444 start to “feel” the normal and shear stress field of each other, and interact (e.g. Fueten and Robin  
445 (1992), Zhou and Aydin (2010)). Fig 11a shows a cartoon of normal and shear stresses that arise  
446 from dissolution on two horizontally over-lapping stylolites at a vertical distance  $d$  from each  
447 other, and the expected evolution due to these two stress fields, the normal and the shear:

448           **1. Increased normal stress leading to increased dissolution** (Fig 11a1): increased  
449 compressive normal stress arises near the tip of each stylolite, with a maximum value achieved at  
450 35°-45° from the mean stylolite plane, as indicated by the “heart-shaped” blue region, following  
451 stress calculation for LVR. In case of uniform dissolution along the stylolite one can use the fact  
452 that such an LVR defect induces a stress like an “edge dislocation” (Katsman et al., 2006a), and  
453 use the calculated stress fields (Landau and Lifshitz (1986), p. 114) to conclude that maximum  
454 compressive stress is induced by the tip at 45°. In case of elliptical dissolution the maximum is  
455 found numerically at 35° (Katsman (2010a)). If spaced at a close enough vertical distance,  $d$ ,  
456 stylolites are expected to induce pressure solution in the compressive stress-enhanced region  
457 between them, and thus connect by dissolution. Similar stylolite connections, via curving tips,  
458 were seen by Mardon (1988) in a partially connected network of solution seams. In the  
459 anastomosing networks observed at the Mitzpe Ramon site, curving planes are abundant: at  
460 scales larger than ~2cm, angles between connecting stylolites are small (approach zero - become  
461 parallel), while at smaller scales they are ~80° (Figure 8a). It is important to note that we find no  
462 peak in the probability function of angles around the expected value of 35°-45°. This suggests  
463 that there might be another process controlling stylolitic connections, possibly formation of shear  
464 or Mode-I fractures that link adjacent stylolites, or connection by „cannibalism’ of long parallel  
465 stylolites, as detailed below.

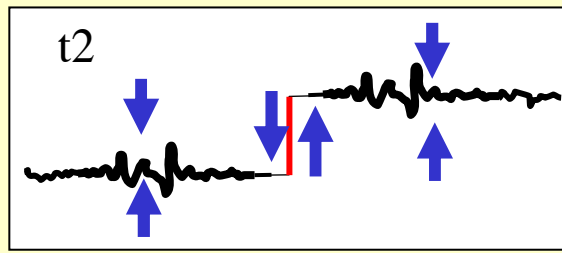
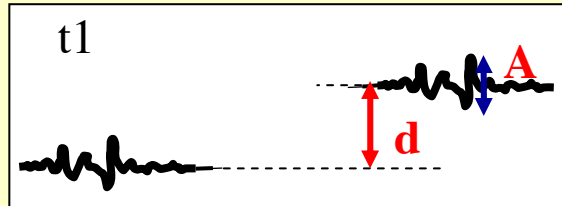
466           **2. Increased shear strain region leading to connection of stylolites by a shear fracture**  
467 (Fig 11a2): In addition to compressive stress, any LVR defect - like the analogous “edge  
468 dislocation” - is calculated theoretically to induce shear stresses near its tip in the plane normal to  
469 it (Landau and Lifshitz (1986), p. 114). The stresses are linearly proportional to the amount of  
470 volume removal (in this case amount of dissolution), and decay as 1/distance from the tip. The  
471 fact that shear stress is induced by a stylolite tip can also be understood intuitively: Two  
472 offsetting stylolites may be viewed as analogs to offset mid-ocean ridges, but with an opposite  
473 sign. While mid-ocean ridges are spreading centers that create rock, stylolites are converging



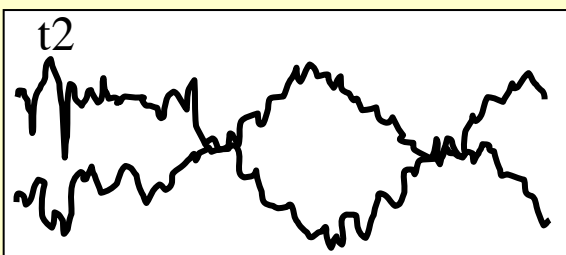
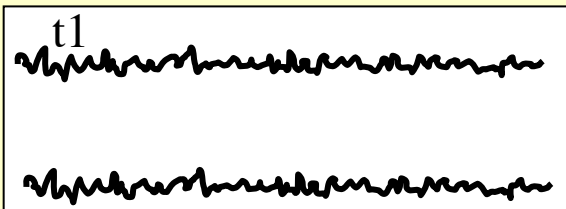
**(a1) connection of isolated stylolites by increased dissolution**



**(a2) connection of isolated stylolites by mode II fractures**



**(b) Connection of long-parallel stylolites**



**(c) Connection by mode I fractures**

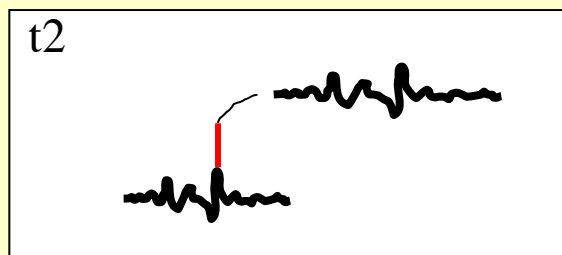
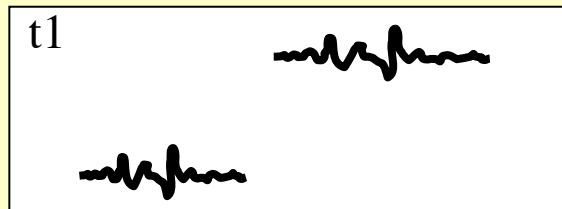


**Fig 11:**

Cartoon showing several possible mechanisms for the formation of interconnected stylolite networks from time t1 to t2.

(a) *Connection of isolated stylolites.*

Increased normal stress (in blue-heart-shaped-regions) enhances dissolution and may change propagation direction (a1), while increased shear strain may cause fracturing (a2). This depends on the mechanical properties of the rock at that time. A and d (a2) control whether there will be connection by linkage or fracturing. Blue arrows (a2) show stress direction.

(b) *Connection of long-parallel stylolites by their dissolution and roughening (“cannibalism” of closely spaced long-parallel stylolites).*

(c) *Connection of stylolites via mode I fractures, emanating from stylolite teeth.* Such fractures can connect stylolites according to both models (a) and (b) (connection of single stylolites or continued dissolution of parallel stylolites). Tips of an adjacent stylolite may curve towards such vein, which induces extensive strain. This scenario fits with stylolite localizing via high

474 centers that destroy/dissolve rock (Peacock and Sanderson, 1995). When spreading/converging  
475 centers are positioned at an offset, they produce shear strain between them, proportional to the  
476 amount of rock created/destroyed. When the shear stress exceeds the material strength, a transfer  
477 fault will form and connect the two stylolites, similar to transform faults that connect offsetting  
478 mid-ocean ridges. “Pull-aparts” are common features in these transfer/transform faults, as seen in  
479 Fig 9a and discussed by Peacock and Sanderson (1995).

480 Two competing processes thus occur between “properly” oriented offset neighboring  
481 growing stylolites: shear fracturing between them due to increased shear stress, and dissolution  
482 due to increased normal stress. The two types of network stylolite populations (interconnected  
483 stylolites and stylolites and fractures) differ in the dominant mechanism: when shear fracturing  
484 dominates, stylolites and fractures will form; when dissolution dominates, interconnected  
485 stylolites form. Whether one mechanism prevails over the other may be associated with the  
486 hydrological state of the rock at the time of deformation: dissolution requires water at the grain  
487 contacts and a fluid path for solute to migrate or diffuse through. Alternatively, the control on  
488 which mechanism dominates may be related to the mechanical strength of the rock at the  
489 overlapping region, which in turn is controlled, *inter alia*, by rock composition, porosity and  
490 local defects.

491  
492 **(ii) Connection of stylolite tips with Mode I cracks (Fig 11b):** The 2<sup>nd</sup> process by which  
493 isolated or planner stylolites may form networks, involves interaction between a stylolite and a  
494 Mode I vein. Mode I veins are often associated with stylolites (Rye and Bradbury, 1988, Smith,  
495 2000, Eren, 2005) and several mechanisms have been suggested to explain their common  
496 appearance perpendicular to compression, i.e. at 90 degrees to stylolites (e.g. Fig 9b, 9d):  
497 concentrated compressive stress at tips of stylolite teeth (Zhou and Aydin, 2010); high fluid pore  
498 pressure within stylolites (Eren, 2005); and extensional stress in the mid-section of stylolites  
499 (Katsman, 2010). Regardless of its formation mechanism, a vein will impact stress-enhanced

500 dissolution in its vicinity, both by enhancing fluid-mediated solute transport (via flow and/or  
501 diffusion), and by perturbing the stress field (Renard et al., 2000a, Renard et al., 2000b).  
502 According to the stress fields (Landau and Lifshitz (1986), p. 114) both opening and Mode II  
503 fractures are expected at certain regions around a stylolite tip, but  $180^\circ$  between stylolites and  
504 veins is not expected from the stress fields, since compactive features such as stylolites induce  
505 compressive stress perpendicular to their plane (Fletcher and Pollard, 1981, Katsman et al.,  
506 2006a) while veins induce exactly the opposite- extension perpendicular to their opening  
507 direction.

508 Stress fields alone may thus not suffice to explain all vein -stylolite attraction, e.g. such as  
509 the interaction in Fig 9b. It is possible to attribute some of the attraction to connectivity and  
510 availability of fluid in veins, that allows fluid enhanced dissolution to dominate the location and  
511 direction of stylolite propagation (e.g. (Renard et al., 2000a, Renard et al., 2000b, Aharonov and  
512 Katsman, 2009). This suggests that the connectivity of stylolites and their ability to transfer  
513 solute in fluid may dominate, at least in some cases, their growth and propagation. The fact that  
514 fluid flow pathways, specifically cracks, enhance pressure solution rates has been observed also  
515 in experiments (Gratier et al., 2009, Croize et al., 2010).

516

517 *(iii) Connection of long parallel stylolites* is the third possibility for formation of  
518 interconnected stylolite networks (Fig 11c). Continued dissolution and roughening of essentially  
519 2D stylolites can result in two stylolites merging in the  $3^{\text{rd}}$  bedding perpendicular, direction, at  
520 least along a limited segment (e.g. Fig 9c). Islands in this case are formed as leftover untouched  
521 regions between coalescing initially self-affine surfaces. In a somewhat similar physical picture  
522 (fracture fronts), where self-affine surfaces „eat each other’ (cannibalism) and by this merge in  
523 places, it was shown that island-scaling is related to the Hurst exponent of the merging surfaces  
524 (Maloy et al., 2005, Maloy et al., 2006, Tallakstad et al., 2011). Comparison between the scaling  
525 of islands and the Hurst exponent of the stylolites may aid in constraining the physical process

526 for network growth, and in understanding why the power-law relating out-of-plane and in-plane  
527 dimensions of islands is characterized by an exponent  $\alpha \approx 0.67$ , similar to the Hurst exponent of  
528 single stylolites, as reported e.g. by Ebner et al. (2009a); Koehn et al. (2007); Laronne Ben-  
529 Itzhak et al. (2012); and Rolland et al. (2012).

530 Connection angles could be used to distinguish whether connectivity occurred by isolated  
531 stylolites meeting at tips or via long stylolites “cannibalizing” each other: If stylolites are  
532 infinite- long- roughening- planes cannibalizing each other, connection angles are expected to be  
533 random, since the geometry of a stylolite at any given point (away from its tip) can be assumed  
534 to be independent of the geometry of the stylolites above and below it at the merging point.  
535 Alternatively, if stylolites connect at tips, connection angles are expected to be  $\sim 35^\circ$ - $45^\circ$  if  
536 connection is by dissolution (Katsman, 2010), or  $\sim 90^\circ$  if by a series of micro-fractures or by  
537 larger-scale fractures (Kaduri, 2013). In our case-studies connections are close to  $90^\circ$  at small  
538 scales, but present a large variability around this value (inset in Fig 7a), which suggests that  
539 micro-fractures are probably involved yet that both mechanisms are plausible.

540

#### 541 **4.2 Strain accommodated by stylolite networks**

542 The dissolution on stylolites introduces an irreversible volume loss in the direction  
543 perpendicular to the stylolite, which produces a compactive strain. In the section below we  
544 attempt to determine the amount of strain accommodated by the three types of stylolite  
545 connectivity classes. The large-scale connections between stylolites and veins are shown to be  
546 important in allowing strain accommodation.

547

##### 548 **Isolated stylolites populations**

549 Isolated stylolites can accommodate a finite and small amount of dissolution before  
550 connecting by dissolution or by shear fractures. Thus, although isolated stylolites may be

551 considered a distinct population in terms of their connectivity and percolation behavior, they are  
552 most likely an intermediate feature in terms of strain. Isolated stylolites most likely eventually  
553 develop into an anastomosing network. The evolutionary picture is expected to be complex since,  
554 assuming that stylolite growth is solute-transfer-limited (as suggested by vein-tips attracting  
555 stylolite-tips in this study, and as seen in some experiments, e.g. Renard et al. (2000b), Zhang  
556 and Spiers (2005) and Zubtsov et al. (2005), Gratier et al. (2009)), then lack of connectivity at  
557 initial stages slows growth of isolated stylolites relative to connected ones. This can explain the  
558 scarcity of observations of isolated **well-developed** stylolites, while pressure solution seams,  
559 which are often considered “baby- stylolites”, are indeed found in isolated populations (Mardon,  
560 1988, Nenna and Aydin, 2011).

561

### 562 *Long, parallel stylolite populations*

563 Dissolution starts on an initially flat plane, which is most often a bedding plane that  
564 progressively roughens with time. The roughness is self-affine and the upper cutoff for self-  
565 affinity grows with time (e.g. Ebner et al. (2009a); Koehn et al. (2007)). The amount of  
566 dissolution,  $U$ , is often estimated from maximum teeth height,  $A_{max}$ , but can also be estimated  
567 from other statistical parameters of the surface (Laronne Ben-Itzhak et al., 2012), provided these  
568 are measured on scales greater than the upper limits of this self-affinity. Estimates derived from  
569 scales smaller than the upper limit for self-affinity (~50cm in the Blanche stylolites)  
570 underestimate dissolution. Compactive vertical strain is calculated from the average amount of  
571 dissolution on stylolites,  $\langle U \rangle$ , and the average spacing between neighboring stylolites  $\langle d \rangle$ ,

572 according to:  $\varepsilon_v = \frac{\langle U \rangle}{\langle d \rangle}$  The amount of dissolution,  $U$ , can also be estimated from seam  
573 thickness (e.g. Tada and Siever (1989)) assuming that initial clay content was uniform, a  
574 questionable assumption if dissolution started on a clay rich bed (Heald, 1955, 1956, Engelder  
575 and Marshak, 1985, Marshak and Engelder, 1985, Aharonov and Katsman, 2009).

576

577 *Anastomosing stylolites*

578 Strain in a section containing this type of stylolite population may be measured in one of two  
579 ways, as from the long parallel stylolites: either from their seam thickness or from their statistical  
580 characteristics. Yet understanding how to use the statistical characteristics (such as Fig 7) to  
581 estimate the amount of dissolution, depends on the network formation which was discussed  
582 above (Aharonov et al., 2010, Aharonov et al., 2011).

583

584 *Stylolite-fracture networks*

585 Strain in this network is shared between the stylolites and the fractures, with Mode I and  
586 Mode II fractures taking different roles. Similar to their large-scale analog, mid-ocean ridges,  
587 **Shear fractures** have an important role in accommodating the compaction strain, even on the  
588 scale of a basin. Pull-aparts can be used here to estimate the compactive strain.

589 **Opening veins** play a more complicated role. Veins appear in two main directions, parallel  
590 and perpendicular to the main compression (Fig 8). The opening veins perpendicular to the  
591 stylolites (as discussed above) play an important, though indirect, role in compaction, by  
592 allowing fluid flow pathways and promoting rapid dissolution and compaction. In contrast,  
593 examples for local extensional strain features found in a direction *parallel to the general*  
594 *compaction direction* are shown in Fig 9e and also evident by the statistically significant  
595 population of stylolite-parallel Mode I fractures (Fig 8). There may be several explanations for  
596 these horizontal veins, and the understanding is made complicated by the fact that we do not  
597 know the timing of the fractures: If they are coeval with the stylolites, they may have developed  
598 due to small block rotations during the development of the stylolites, or due to local extensive  
599 strain. Some wing-crack fractures may also have developed at a different time than the stylolites,  
600 associated with a micro thrust fault under the effect of a tectonic horizontal contraction. Time  
601 scales may also be different for the two processes: fracturing may be a fast process, while

602 pressure solution a slow one. This difference in timescales is also very interesting to study.  
603 However, since we do not have any information on the tectonic context of this slab (the exact  
604 location of the quarry from which it was taken is unknown), we cannot have more than these  
605 speculations.

606

### 607 **4.3 Stylolites and fluid flow**

608 The effects of stylolites on flow have been discussed previously (Wong and Oldershaw,  
609 1981, Carozzi and Vonbergen, 1987, Rye and Bradbury, 1988, Tada and Siever, 1989, Finkel  
610 and Wilkinson, 1990, Raynaud and Carrioschaffhauser, 1992, Corwin et al., 1997, Ehrenberg,  
611 2006, Heap et al., 2014). Yet the question of their connectivity, which is crucial for fluid flow,  
612 has not been discussed. Two very different aspects are important with regards to fluid flow. The  
613 first is the interaction between fluid-flow and stylolites **during** their formation; while the second  
614 is the influence of stylolite populations on fluid flow in the crustal rocks in which they are  
615 present, long **after** their formation. We address both aspects here, as we believe that the approach  
616 presented in this paper is an important step in their understanding.

617

#### 618 **4.3.1 Interaction between fluid-flow and stylolites during their formation:**

619 Fractures were shown to be intimately related to stylolites in the Umbria-Marche slab  
620 (Fig 9). Some Mode I cracks are clearly formed with the stylolites (Figs 9a, 9b and 9f) while  
621 others are less clearly timed (Figs 9d and 9e). Mode I fractures that seem coeval with the  
622 stylolites have affected the growth of stylolites by diverting their average plane direction (Figs  
623 9b1 and 9b2). This interaction could perhaps be explained if their presence enhanced solute  
624 transport rates and also extended the volume available for precipitation of the dissolved matter,  
625 before they were filled with precipitation. Stylolites probably also affected fracture formation, as  
626 indicated by the latter originating from stylolite teeth, from the tapering of fractures away from

627 stylolites, and from shear fractures connecting stylolites. Therefore stylolites and fractures have a  
628 mutual effect on each other in our case study. This symbiosis affects simultaneously the amount  
629 of compactive strain that may occur in the system (see section 4.2), the pattern of fluid flow in  
630 the system, and the locations of dissolution and precipitation. In a system containing very little or  
631 no fractures (such as the long-parallel stylolites in the Blanche cliff), at least part of the  
632 precipitation of the dissolved matter on the stylolites occurred in the adjacent porosity (as shown  
633 in thin-sections in Laronne Ben-Itzhak et al. (2012)). In that site, measurements suggested a  
634 scenario whereby the dissolution-precipitation process may have stopped once this porosity was  
635 occluded, so that shutting down precipitation or diffusion in pores limited the amount of  
636 dissolution that occurred (Laronne Ben-Itzhak et al., 2012). However, in a system that contains  
637 many fractures, and could also be considered an open system, there is less constraint on the  
638 amount of dissolution-driven compactive strain the system can undergo.

639

#### 640 ***4.3.2 Interaction between fluid-flow and stylolites after their formation:***

641 Different percolation geometries of stylolites are each accompanied by associated  
642 percolation geometries of the host rock: zero-connectivity of stylolites (isolated) comes together  
643 with a fully percolated rock-body. 2D percolation of stylolites (long-parallel class) comes  
644 together with parallel percolation of the rock-body between the stylolites but allows no  
645 percolation in the bedding -perpendicular direction. 3D percolation of anastomosing networks  
646 causes disconnected lenses of rock. It is important to recall that this percolation approach and the  
647 division to stylolite connectivity-classes do not infer that stylolites are necessarily channels to  
648 fluids. Stylolites may be of higher permeability than the rock-body regions between them (e.g.  
649 Wong and Oldershaw (1981); Carozzi and Vonbergen (1987); [ENREF 68](#) Carrio-Schaffhauser  
650 et al. (1990); Raynaud and Carrioschaffhauser (1992); Heap et al. (2014);). But the opposite may  
651 also exist in some cases: stylolites can be low-permeability features, due to the highly-cemented  
652 regions often observed around stylolites (Corwin et al. (1997); Ehrenberg (2006)).



653 The connectivity is important both when stylolites act as flow conduits, and when they act as  
654 barriers:

655 **I: Isolated stylolites – no percolation:** If stylolites have well defined tips and do not touch each  
656 other, the system is below the percolation threshold, and their permeability shouldn't affect the  
657 rock body too much, even if it is different than the permeability of the host rock.

658 **II: Parallel stylolites - 2D percolation:** These may induce anisotropic permeability. If they are  
659 more permeable than the host rock permeability will be enhanced in the surface-parallel direction  
660 but not in the perpendicular direction. Instead, if stylolites have lower permeability than the host  
661 rock they will not affect the surface-parallel direction yet will act as barriers in the perpendicular  
662 direction.

663 **III: Stylolite Networks - 3D percolation:** In this case the stylolites percolate but the rock body  
664 lenses are disconnected from each other. Highly permeable stylolites will enhance flow in a more  
665 or less isotropic manner, while low permeability stylolites will create a well-connected system of  
666 barriers, expected to reduce permeability of the rock.

667

## 668 **5. Summary and conclusions**

669 Our interest in large scale pressure solution structures, and fluid flow and strain in stylolitic  
670 rocks, led us to suggest a classification of stylolite populations in the field, based on their  
671 network connectivity. Fieldwork and percolation theory guided us to classify three distinct  
672 groups: *isolated stylolites*, *long bedding-parallel stylolites* and *interconnected networks of*  
673 *stylolites*. Isolated stylolites were previously quantified. The other two populations are quantified  
674 here for the first time.

675 Measurements conducted to characterize very *long bedding-parallel stylolites* show that their  
676 geometrical characteristics (e.g. maximum amplitude) are fairly constant along their length.  
677 Observations reported here and in Laronne Ben-Itzhak et al. (2012) support a model of formation

678 by roughening caused by dissolution localized on preexisting planes, most often bedding planes,  
679 (Renard et al., 2004, Schmittbuhl et al., 2004, Koehn et al., 2007, Ebner et al., 2009a). The  
680 localization mechanism for uniform dissolution on very large bedding- planes is not strictly  
681 known, but is likely connected to initial bedding-related compositional heterogeneity (possibly  
682 higher clay content) (Lind, 1993), implying that stress may not be the only (nor the most  
683 important) drive for their formation.

684 The interconnected networks of stylolites are further divided into *networks of anastomosing*  
685 *stylolites* and *stylolites-fracture networks*. *Networks of anastomosing stylolites* show islands,  
686 with a self-similar shape, bounded by stylolite seams. Connection angles between stylolites in the  
687 network average ~90 degrees near the meeting point, while stylolites become parallel at larger  
688 scales. The *Interconnected networks of stylolites and fractures*, which are composed of both  
689 Mode I and II fractures connecting stylolites, show that most fractures are perpendicular to  
690 stylolites. The measurements on both types of interconnected networks, together with small-scale  
691 observations of field relations between stylolites and fractures, suggest the possibility of several  
692 formation mechanisms for stylolite networks: (1) connection of tips of active isolated stylolites;  
693 (2) connection (via cannibalization) of long parallel stylolites; and (3) connection of stylolite tips  
694 with Mode I cracks. However full understanding of these mechanisms and when each one  
695 operates needs further work.

696 The measurements and analysis presented in this manuscript have several important  
697 implications. The first is that stylolites may form by various mechanisms. This is implied from  
698 the recognition that there are different geometries with different characteristics of stylolite  
699 populations. In some cases stylolites may propagate laterally during dissolution, while in others  
700 the in-plane distribution is set from the beginning. A second conclusion is that stylolites and  
701 veins often co-exist in a geometry which indicates that they interact with one another. Stylolites  
702 may induce stress perturbations that govern the location of fractures (emanating from their teeth  
703 or edges). Fractures affect stylolites (by diverting their mean direction) possibly due to the

704 increased solute transport that they allow. The two processes may have widely different time  
705 scales –fractures are often fast while stylolites dissolve slowly. The intriguing interactions affect  
706 both the strain and the fluid flow pathways, although quantification and full understanding need  
707 further field, modeling, and lab work.  
708

709 **Acknowledgments**

710 This research was sponsored by ExxonMobil and by an ISF grant #751/08. We deeply thank

711 Yehuda Eyal, Eitan Sass and the late and beloved Hagai Ron, for sharing with us their

712 knowledge and experience in the field, and for showing us many of the field locations. EA and

713 RT acknowledge the support of the Marie Curie ITN Flowtrans.

714

715 **Figure Captions**

716

717 **Figure 1:** Long parallel stylolites in the Blanche cliff, Northern Israel (adapted from Figure 1 in  
718 Ben-Itzhak et al. (2012)).

719 **(a)** Part of the cliff with four stylolites (labeled „4(19)’, „5(7)’, „5(9)’ and „5(13)’ in Figure 5b)  
720 marked in red, showing they can be traced for a large distance.

721 **(b)** Zoom on two other stylolites („3(10)’ marked by a green arrow, and „3(11)’, see Figure 5b),  
722 where stylolite cm-scale roughness is evident.

723

724 **Figure 2:** Interconnected stylolite network from a Cenomanian limestone quarry near Mitzpe  
725 Ramon, Southern Israel (site 2, Table 1).

726 **(a)** Large scale photo and **(b)** zoom of the mapped exposure, studied from two perpendicular  
727 sides. High-resolution photographs were combined using a grid for digitization of the stylolite  
728 network (the black grid in (a) was drawn on the photo to illustrate where the actual grid on the  
729 exposure was marked).  $5.5 \times 1.2 \text{ m}^2$  were mapped on either of the two perpendicular sides.

730

731 **Figure 3:** Three scales of a digitized map of the interconnected stylolite network seen in Figure 2  
732 (the right section of the two perpendicular exposures in Figure 2). Regions between connected  
733 stylolites are termed “islands”, and are described by several parameters: island area  $S$ ; connection  
734 angle  $\theta$  between stylolite segments of length  $L$ ; and a bounding rectangle with bedding-parallel  
735 and bedding perpendicular dimensions  $\xi_{\parallel}$  and  $\xi_{\perp}$ , respectively.

736

737 **Figure 4:** Interconnected network of stylolites and fractures in limestone (Calcare Massiccio  
738 Formation, Jurassic, Italy).

739 **(a)** Close-up photo showing interacting stylolites and fractures; and

740 **(b)** Larger scale digitized map of major and minor stylolites (pink and green, respectively) and of  
741 fractures (blue).

742

743 **Figure 5:** Images showing the Blanche (Ein El-Assad Fm.) section in the northern part of the  
744 cliff, where all 65 stylolites were identified and measured.

745 **(a)** The section was divided to 9 major units differentiated by major stylolites (in orange). Most  
746 of the measurements were performed in the parts that are marked in white (these are the same  
747 units as in the orange-part but on a closer and more accessible cliff).

748 **(b)** Zoom on rectangle in (a). Stylolites are labeled according to their vertical position within a  
749 unit, i.e., 5(3) is the third stylolite from the bottom of unit 5. Spacing between neighboring  
750 stylolites (5(12) and 5(13), as an example) is displayed in white.

751

752 **Figure 6:** Measurements conducted on long parallel stylolites at several locations along the  
753 ~1km – long Blanche cliff.

754 **(a)** Spacing between three couples of stylolites.

755 **(b)** and **(c)** Maximum teeth amplitude ( $A_{\max}$ ) of six different stylolites (viewed in two separate  
756 graphs only for purposes of convenience). Error bars are the standard deviation of several  
757 measurements in each location. No trend in spacing or  $A_{\max}$  along the length of the stylolites is  
758 identified.

759

760 **Figure 7:** Statistical analysis on variables illustrated in Figure 3c, performed in Mitzpe Ramon  
761 quarry.

762 **(a)** angle between adjacent stylolites as function of distance from junction,  $\theta(L)$ , measured at all  
763 stylolite junctions. Each data point is the average of all  $\theta(L_i)$  in the exposure, where  $i$  is the index  
764 of the junction. Error bars are standard deviation. Both are acquired from normal distribution  
765 functions produced for each  $L_i$ . The inset is such an example distribution for  $L=0.9\text{cm}$ .

766 **(b)** Island heights  $\xi_{\perp}$  versus island width  $\xi_{\parallel}$  measured on all islands in the outcrop, as explained  
767 in the text. The line is a best fit to the correlation between  $\xi_{\perp}$  and  $\xi_{\parallel}$ .

768

769 **Figure 8:** Orientations of stylolites and fractures in the Umbria–Marche slab, Apennines  
770 (analyzed upon map in Fig 4b).

771 H indicates horizontal (bedding parallel) and V indicates vertical. Red indicates the stylolite  
772 population orientation and blue the fracture orientations.

773

774 **Figure 9:** Zoom-in on the slab of Figure 4 showing small-scale field-relations between fractures  
775 and stylolites and between the stylolites themselves.

776 **(a)** Mode II fracture with pull-apart structure filled with cement connecting two stylolites.  
777 Interpreted strain direction is marked by arrows.

778 **(b1)** and **(b2)** Two examples of Mode I veins sub-parallel to the stylolite teeth and splaying from  
779 them. The veins are commonly triangular, with the aperture being largest close to the stylolite  
780 surface (b1). Stylolite mean direction is changed near a vein (circled regions).

781 (c) Interconnected stylolite network that seems to be derived from stylolite “cannibalism” (see  
782 text for further explanation).

783 (d) Complex connection between non-overlapping stylolites by an array of oblique veins.

784 (e) Veins parallel to stylolite surface mean direction. This population of fractures parallel to  
785 stylolites is statistically common (see Figure 8). The formation of these wing-crack fractures may  
786 be explained in several ways (see discussion in text).

787 (f) Vein and stylolites closely interacting.

788 Possible mechanisms for the formation of the observations in Figures 9a, 9b and 9c, appear in  
789 Figures 11a, 11b and 11c, respectively.

790

791 **Figure 10:** Connectivity/percolation-based classification of sedimentary stylolite populations: (a)  
792 Isolated stylolites; (b) Long bedding-parallel stylolite population; and (c) Interconnected-  
793 network stylolite population, further divided into (c1) anastomosing networks of stylolites and  
794 (c2) interconnected networks of stylolites and fractures (fractures appear in blue).

795

796 **Figure 11:** Cartoon showing several possible mechanisms for the formation of interconnected  
797 stylolite networks between times  $t_1$  and  $t_2$ .

798 (a) *Connection of isolated stylolites.* Increased normal stress (in blue-heart-shaped-regions)  
799 enhances dissolution and may change propagation direction (a1), while increased shear strain  
800 may cause fracturing (a2). This depends on the mechanical properties of the rock at that time.  $A$   
801 and  $d$  (a2) control whether there will be connection by linkage or fracturing. Thick blue arrows  
802 (a2) show stress direction.

803 (b) *Connection of stylolites via mode I fractures,* emanating from stylolite teeth. Tips of an  
804 adjacent stylolite may curve towards such vein, which induces extensive strain. This scenario fits  
805 with stylolite localizing via high dissolution rates. Rapid dissolution in diffusion limited systems  
806 can be induced by rapid fluid pathways.

807 (c) *Connection of long-parallel stylolites* by their dissolution and roughening (“cannibalism” of  
808 closely spaced long-parallel stylolites).

809

811 **Reference List**

812

- 813 Aharonov, E., Katsman, R. 2009. Interaction between Pressure Solution and Clays in Stylolite  
814 Development: Insights from Modeling. *American Journal of Science* **309**(7), 607-632.
- 815 Aharonov, E., Katsman, R., Laronne Ben-Itzhak, L. 2010. How do stylolite networks and  
816 stylolite-fracture networks form: insights from modeling. In: *28th IUGG Conference on*  
817 *Mathematical Geophysics*, Pisa, Italy.
- 818 Aharonov, E., Laronne Ben-Itzhak, L., Katsman, R., Karcz, Z., Kaduri, M. 2011. Stylolite  
819 Populations in Limestone: Field observations and formation models, Abstract T33C-  
820 2427. In: *AGU fall meeting*, San Francisco.
- 821 Alvarez, W., Engelder, T., Geiser, P. A. 1978. Classification of Solution Cleavage in Pelagic  
822 Limestones. *Geology* **6**(5), 263-266.
- 823 Andrews, L. M., Railsback, L. B. 1997. Controls on stylolite development: Morphologic,  
824 lithologic, and temporal evidence from bedding-parallel and transverse stylolites from the  
825 US Appalachians. *Journal of Geology* **105**(1), 59-73.
- 826 Benedicto, A., Schultz, R. A. 2010. Stylolites in limestone: Magnitude of contractional strain  
827 accommodated and scaling relationships. *Journal of Structural Geology* **32**, 1250-1256.
- 828 Bour, O., Davy, P. 1998. On the connectivity of three-dimensional fault networks,. *Water*  
829 *Resources Research* **34**(10), 2611-2622.
- 830 Bunde, A., Havlin, S. 1991. Fractals and disordered systems (edited by Bunde, A. & Havlin, S.).  
831 Springer-Verlag New York, Inc., 350.
- 832 Carozzi, A. V., Vonbergen, D. 1987. Stylolitic Porosity in Carbonates - a Critical Factor for  
833 Deep Hydrocarbon Production. *Journal of Petroleum Geology* **10**(3), 267-282.
- 834 Carrio-Schaffhauser, E., Raynaud, S., Latière, H. J., Mazerolle, F. 1990. Propagation and  
835 localization of stylolites in limestones. *Geological Society, London, Special Publications*  
836 **54**(1), 193-199.
- 837 Cartwright, J. A., Trudgill, B. D., Mansfield, C. S. 1995. Fault growth by segment linkage: an  
838 explanation for scatter in maximum displacement and trace length data from the  
839 Canyonlands Grabens of SE Utah. *Journal of Structural Geology* **17**(9), 1319-1326.
- 840 Cello, G. 1997. Fractal analysis of a Quaternary fault array in the central Apennines, Italy.  
841 *Journal of Structural Geology* **19**(7), 945-963.
- 842 Corwin, L. W., Broomhall, R. W., Saidikowski, R. M., Wooten, J. N. 1997. Stylolites Impact the  
843 Miscible Nitrogen Flood in a Mature Carbonate Oil Field. *SPE International, Inc.*, **37780**,  
844 213-221.
- 845 Croize, D., Renard, F., Bjorlykke, K., Dysthe, D. K. 2010. Experimental calcite dissolution  
846 under stress: Evolution of grain contact microstructure during pressure solution creep.  
847 *Journal of Geophysical Research-Solid Earth* **115**.
- 848 Dawers, N. H., Anders, M. H., Scholz, C. H. 1993. Growth of normal faults - displacement-  
849 length scaling. *Geology* **21**(12), 1107-1110.
- 850 Deboer, R. B. 1977. Thermodynamics of Pressure Solution - Interaction between Chemical and  
851 Mechanical Forces. *Geochimica Et Cosmochimica Acta* **41**(2), 249-256.
- 852 Ebner, M., Koehn, D., Toussaint, R., Renard, F. 2009a. The influence of rock heterogeneity on  
853 the scaling properties of simulated and natural stylolites. *Journal of Structural Geology*  
854 **31**(1), 72-82.
- 855 Ebner, M., Koehn, D., Toussaint, R., Renard, F., Schmittbuhl, J. 2009b. Stress sensitivity of  
856 stylolite morphology. *Earth and Planetary Science Letters* **277**(3-4), 394-398.
- 857 Ehrenberg, S. N. 2006. Porosity destruction in carbonate platforms. *Journal of Petroleum*  
858 *Geology* **29**(1), 41-51.



- 859 Engelder, T., Marshak, S. 1985. Disjunctive cleavage formed at shallow depths in sedimentary  
860 rocks. *Journal of Structural Geology* **7**(3/4), 327-343.
- 861 Eren, M. 2005. Origin of stylolite related fractures in atoka bank carbonates, eddy county, New  
862 Mexico, USA. *Carbonates and Evaporites* **20**(1), 42-49.
- 863 Finkel, E. A., Wilkinson, B. H. 1990. Stylolitization as Source of Cement in Mississippian  
864 Salem Limestone, West-Central Indiana. *Aapg Bulletin-American Association of*  
865 *Petroleum Geologists* **74**(2), 174-186.
- 866 Fletcher, R. C., Pollard, D. D. 1981. Anti-Crack Model for Pressure Solution Surfaces. *Geology*  
867 **9**(9), 419-424.
- 868 Fueten, F., Robin, P. Y. F. 1992. Finite-Element Modeling of the Propagation of a Pressure  
869 Solution Cleavage Seam. *Journal of Structural Geology* **14**(8-9), 953-962.
- 870 Gratier, J.-P., Guiguet, R., Renard, F., Jenatton, L., Bernard, D. 2009. A pressure solution creep  
871 law for quartz from indentation experiments. *Journal of Geophysical Research: Solid*  
872 *Earth* **114** B03403.
- 873 Greene, G. W., Kristiansen, K., Meyer, E. E., Boles, J. R., Israelachvili, J. N. 2009. Role of  
874 electrochemical reactions in pressure solution. *Geochimica Et Cosmochimica Acta*  
875 **73**(10), 2862-2874.
- 876 Gruzman, Y. 1997. Origin of sedimentary stylolites from Israel. Unpublished M.Sc thesis,  
877 Hebrew University.
- 878 Gupta, A., Scholz, C. H. 2000. A model of normal fault interaction based on observations and  
879 theory. *Journal of Structural Geology* **22**(7), 865-879.
- 880 Guzzetta, G. 1984. Kinematics of stylolite formation and physics of pressure-solution process.  
881 *Tectonophysics* **101**, 383-394.
- 882 Heald, M. T. 1955. Stylolite in sandstones. *The Journal of Geology* **63**(2), 101-114.
- 883 Heald, M. T. 1956. Cementation of Simpson and St. Peter sandstones in parts of Oklahoma,  
884 Arkansas and Missouri. *The Journal of Geology* **64**(1), 16-30.
- 885 Heap, M. J., Baud, P., Reuschlé, T., Meredith, P. G. 2014. Stylolites in limestones: Barriers to  
886 fluid flow? *Geology* **42**(1), 51-54.
- 887 Hickman, S. H., Evans, B. 1995. Kinetics of Pressure Solution at Halite-Silica Interfaces and  
888 Intergranular Clay Films. *Journal of Geophysical Research-Solid Earth* **100**(B7), 13113-  
889 13132.
- 890 Kaduri, M. 2013. Interconnected Stylolite Networks: field observations, characterization, and  
891 modeling, M.Sc. thesis, The Hebrew University.
- 892 Kaplan, M. Y. 1976. Origin of stylolites. *Doct. Acad. Sci USSR, Earth Sci. Sect.* **221**, 205-7.
- 893 Karcz, Z., Scholz, C. H. 2003. The fractal geometry of some stylolites from the Calcare  
894 Massiccio Formation, Italy. *Journal of Structural Geology* **25**(8), 1301-1316.
- 895 Katsman, R. 2010. Extensional veins induced by self-similar dissolution at stylolites: analytical  
896 modeling. *Earth and Planetary Science Letters* **299**, 33-41.
- 897 Katsman, R., Aharonov, E. 2005. Modelling localized volume changes: Application to pressure  
898 solution and stylolites. *Geochimica Et Cosmochimica Acta* **69**(10), A312-A312.
- 899 Katsman, R., Aharonov, E., Scher, H. 2006a. Localized compaction in rocks: Eshelby's  
900 inclusion and the Spring Network Model. *Geophysical Research Letters* **33**(10).
- 901 Katsman, R., Aharonov, E., Scher, H. 2006b. A numerical study on localized volume reduction  
902 in elastic media: Some insights on the mechanics of anticracks. *Journal of Geophysical*  
903 *Research-Solid Earth* **111**(B3).
- 904 Koehn, D., Ebner, M., Renard, F., Toussaint, R., Passchier, C. W. 2012. Modelling of stylolite  
905 geometries and stress scaling. *Earth and Planetary Science Letters* **341-34**. 771-704 ,4
- 906 Koehn, D., Renard, F., Toussaint, R., Passchier, C. W. 2007. Growth of stylolite teeth patterns  
907 depending on normal stress and finite compaction. *Earth and Planetary Science Letters*  
908 **257**(3-4), 582-595.

- 909 Landau, L. D., Lifshitz, E. M. 1986. *Theory of Elasticity: Vol. 7 of Course of Theoretical*  
910 *Physics*. Elsevier Ltd.
- 911 Laronne Ben-Itzhak, L., Aharonov, E., Toussaint, R., Sagy, A. 2012. Upper bound on stylolite  
912 roughness as indicator for amount of dissolution. *Earth and Planetary Science Letters*  
913 **3**,796-786 ,118–17
- 914 Lehner, F. K. 1995. A Model for Intergranular Pressure Solution in Open Systems.  
915 *Tectonophysics* **245**(3-4), 153-170.
- 916 Lind, I. L. 1993. Stylolites in chalk from Leg 130, Ontong Java Plateau. *Proceedings of the*  
917 *Ocean Drilling Program, Scientific Results* **130**, 445-451.
- 918 Main, I. 1996. Statistical physics, seismogenesis, and seismic hazard. *Reviews of Geophysics*  
919 **34**(4), 433-462.
- 920 Maloy, K. J., Santucci, S., Schmittbuhl, J., Toussaint, R. 2006. Local Waiting Time Fluctuations  
921 along a Randomly Pinned Crack Front. *Physical Review Letters* **96**(4), 045501.
- 922 Maloy, K. J., Toussaint, R., Schmittbuhl, J. 2005. Dynamics and structure of interfacial crack  
923 fronts. In: *Proceedings of the ICF11, 11th International Conference on Fracture*, Torino.
- 924 Mardon, D. 1988 .Localized pressure solution and the formation of discrete solution seams.  
925 Unpublished Ph. D. thesis, Texas A&M University.
- 926 Marshak, S., Engelder, T. 1985. Development of Cleavage in Limestones of a Fold-Thrust Belt  
927 in Eastern New-York. *Journal of Structural Geology* **7**(3-4), 345-359.
- 928 McLachlan, D. S., Blaszkiewicz, M., Newnham, R. E. 1990. Electrical Resistivity of  
929 Composites. *Journal of the American Ceramic Society* **73**(8), 2187-2203.
- 930 McLeod, A. E., Dawers, N. H., Underhill, J. R. 2000. The propagation and linkage of normal  
931 faults: insights from the Strathspey-Brent-Statfjord fault array, northern North Sea. *Basin*  
932 *Research* **12**(3-4), 263-284.
- 933 Nenna, F. A., Aydin, A. 2011. The formation and growth of pressure solution seams in clastic  
934 rocks: A field and analytical study. *Journal of Structural Geology* **33**, 633-643.
- 935 Park, W. C., Schot, E. H. 1968. Stylolites - Their Nature and Origin. *Journal of Sedimentary*  
936 *Petrology* **38**(1), 17797-5.
- 937 Paterson, M. S. 1995. A Theory for Granular Flow Accommodated by Material Transfer Via an  
938 Intergranular Fluid. *Tectonophysics* **245**(3-4), 135-151.
- 939 Peacock, D. C. P., Sanderson, D. J. 1995. Pull-Aparts, Shear Fractures and Pressure Solution.  
940 *Tectonophysics* **241**(1-2), 1-13.
- 941 Powell, C. M. 1979. A morphological classification of rock cleavage. *Tectonophysics*  
942 *Microstructural processes during deformation and metamorphism* **58**(1-2), 21-34.
- 943 Railsback, L. B. 1993. Lithologic Controls on Morphology of Pressure-Dissolution Surfaces  
944 (Stylolites and Dissolution Seams) in Paleozoic Carbonate Rocks from the Mideastern  
945 United-States. *Journal of Sedimentary Petrology* **63**(3), 513-522.
- 946 Raynaud, S., Carrioschaffhauser, E. 1992. Rock Matrix Structures in a Zone Influenced by a  
947 Stylolite. *Journal of Structural Geology* **14**(8-9), 973-980.
- 948 Renard, F., Brosse, E ., Gratier, J. P. 2000a. The Different Processes Involved in the Mechanism  
949 of Pressure Solution in Quartz-Rich Rocks and their Interactions. In: *Quartz Cementation*  
950 *in Sandstones* (edited by Worden, R. H. & Morad, S.). Blackwell Publishing Ltd.,  
951 Oxford, UK.
- 952 Renard, F., Dysthe, D., Feder, J., Bjorlykke, K., Jamtveit, B. 2001. Enhanced pressure solution  
953 creep rates induced by clay particles: Experimental evidence in salt aggregates.  
954 *Geophysical Research Letters* **28**(7), 1295-1298.
- 955 Renard, F., Gratier, J. P .,Jamtveit, B. 2000b. Kinetics of crack-sealing, intergranular pressure  
956 solution, and compaction around active faults. *Journal of Structural Geology* **22**(10),  
957 1395-1407.

- 958 Renard, F., Schmittbuhl, J., Gratier, J. P., Meakin, P., Merino, E. 2004. Three-dimensional  
959 roughness of stylolites in limestones. *Journal of Geophysical Research-Solid Earth*  
960 **109**(B3).
- 961 Rolland, A., Toussaint, R., Baud, P., Schmittbuhl, J., Conil, N., Koehn, D., Renard, F., Gratier,  
962 J. P. 2012a. Modeling the growth of stylolites in sedimentary rocks. *Journal of*  
963 *Geophysical Research-Solid Earth* **117**(6), B06403.
- 964 Rye, D. M., Bradbury, H. J. 1988. Fluid-Flow in the Crust - an Example from a Pyrenean Thrust  
965 Ramp. *American Journal of Science* **288**(3), 197-235.
- 966 Safaricz, M. 2002. Pressure solution in chalk. Unpublished Ph.D. thesis, Royal Holloway  
967 University of London.
- 968 Safaricz, M., Davison, I. 2005. Pressure solution in chalk. *Aapg Bulletin* **89**(3), 383-401.
- 969 Schmittbuhl, J., Renard, F., Gratier, J. P., Toussaint, R. 2004. Roughness of stylolites:  
970 Implications of 3D high resolution topography measurements. *Physical Review Letters*  
971 **93**(23).
- 972 Segall, P., Pollard, D. D. 1980. Mechanics of discontinuous faults. *Journal of Geophysical*  
973 *Research* **85**(B8), 4337-4350.
- 974 Shimizu, I. 1995. Kinetics of Pressure Solution Creep in Quartz - Theoretical Considerations.  
975 *Tectonophysics* **245**(3-4), 121-134.
- 976 Sibley, D. F., Blatt, H. 1976. Intergranular Pressure Solution and Cementation of Tuscarora  
977 Orthoquartzite. *Journal of Sedimentary Petrology* **46**(4), 881-896.
- 978 Smith, J. V. 2000. Three-dimensional morphology and connectivity of stylolites hyperactivated  
979 during veining. *Journal of Structural Geology* **22**(1), 59-64.
- 980 Sneh, A., Weinberger, R. 2003. Geological Map of Israel. Sheet 2-II Metulla. Israel Geological  
981 Survey.
- 982 Stockdale, P. B. 1922. Stylolites: their nature and origin. *Indiana University Studies* **9**, 1-97.
- 983 Tada, R., Siever, R. 1989. Pressure Solution During Diagenesis. *Annual Review of Earth and*  
984 *Planetary Sciences* **17**, 89-118.
- 985 Tallakstad, K. T., Knudsen, H. A., Ramstad, T., Løvoll, G., Måløy, K. J., Toussaint, R.,  
986 Flekkøy, E. G. 2009a. Steady-State Two-Phase Flow in Porous Media: Statistics and  
987 Transport Properties. *Physical Review Letters* **102**(7), 074502.
- 988 Tallakstad, K. T., Løvoll, G., Knudsen, H. A., Ramstad, T., Flekkøy, E. G., Måløy, K. J. 2009b.  
989 Steady-state, simultaneous two-phase flow in porous media: An experimental study.  
990 *Physical Review E* **80**(3), 036308
- 991 Tallakstad, K. T., Toussaint, R., Santucci, S., Schmittbuhl, J., Maloy, K. J. 2011. Local  
992 dynamics of a randomly pinned crack front during creep and forced propagation: An  
993 experimental study. *Physical Review E* **83**(4), 046108.
- 994 Thomson, A. 1959. *Pressure solution and porosity*. Soc. Econ. Paleontol. Mineral. Special  
995 publication.
- 996 Vermilye, J. M., Scholz, C. 1995. Relation between vein length and aperture. *Journal of*  
997 *Structural Geology* **17**(3), 423-434.
- 998 Walderhaug, O., Bjorkum, P. A., Aase, N. E. 2006. Kaolin-coating of stylolites, effect on quartz  
999 cementation and general implications for dissolution at mineral interfaces. *Journal of*  
1000 *Sedimentary Research* **76**(1-2), 234-243.
- 1001 Weyl, P. K. 1959. Pressure solution and the force of crystallization: a phenomenological theory.  
1002 *Journal of Geophysical Research-Solid Earth* **64**, 2001-2025.
- 1003 Willemse, E. J. M. 1997. Segmented normal faults: Correspondence between three-dimensional  
1004 mechanical models and field data. *Journal of Geophysical Research -Solid Earth*  
1005 **102**(B1), 675-692.
- 1006 Wong, P. K., Oldershaw, A. 1981. Burial Cementation in the Devonian, Kaybob Reef Complex,  
1007 Alberta, Canada. *Journal of Sedimentary Petrology* **51**(2), 507-520.

1008 Zhang, X., Spiers, C. J. 2005. Compaction of granular calcite by pressure solution at room  
1009 temperature and effects of pore fluid chemistry. *International Journal of Rock Mechanics*  
1010 *and Mining Sciences* **42**(7-8), 950-960.  
1011 Zhou, X., Aydin, A. 2010. Mechanics of pressure solution seam growth and evolution. *Journal*  
1012 *of Geophysical Research-Solid Earth* **115**, 18.  
1013 Zubtsov, S., Renard, F., Gratier, J. P., Dysthe, D. K., Traskine, V. 2005. *Single contact pressure*  
1014 *solution creep on calcite monocrystals*. Geological society Special Publication.  
1015

1016

1017  
1018  
1019  
1020  
1021  
1022  
1023  
1024  
1025  
1026  
1027  
1028